Classification of ignimbrites and their eruptions

Guido Giordano [a,b,*], Ray A.F. Cas [c,d]

[a] Dipartimento di Scienze – Sezione Geologia, Università di Roma Tre, Roma, Italy
[b] Istituto di Geologia Ambientale e Geoingegneria, CNR, 00010 Montelibretti, Italy
[c] School of Earth, Atmosphere and Environment, Monash University, Victoria, Australia
[d] CODES and Earth Science, School of Natural Sciences, University of Tasmania, Australia

ARTICLE INFO

ABSTRACT

The term "ignimbrite" probably encompasses the one of the largest ranges of deposit types on Earth, associated with the partial to total collapse of explosive eruption columns feeding pyroclastic density currents. Surprisingly, there is no quantified classification scheme for ignimbrite types, as there is for fallout deposits, and this is a remarkable deficiency of modern volcanology. This has so far prevented the identification of standardized descriptors for ignimbrites and the improvement of methods for the documentation of their characteristics, such as happened for fallout deposits, building on the classification scheme proposed by Walker in 1973. Despite some earlier attempts, ignimbrite types do not conform to eruption style nomenclature. In this paper, we explore and discuss descriptors for a classification scheme based on the correlation of runout, areal extent, aspect ratio and volume from a compiled database comprising 92 ignimbrites, which then allows current understanding of pyroclastic flow dynamics to be considered. We refer to single ignimbrite outflow units, i.e. emplaced without significant breaks in their sedimentation, in extra-caldera settings and forming individual cooling units, irrespective of internal lithofacies architecture. Our main finding is that ignimbrites show remarkable power-law relationship between dispersal area/equivalent runout and bulk volume. Runout is directly related to increasing mass flow rate feeding the pyroclastic current. Volume is related to the magnitude of the flow event. We therefore propose that by measuring first order field observables such as bulk volume and dispersal area provides the opportunity to evaluate magnitude and intensity of related pyroclastic currents and, for large eruptions dominated by ignimbrites, of the eruption. Based on the relationships identified we propose that ignimbrites that originated from the collapse of single point-source eruption columns, usually smaller than 1 km³, are named "Vulcanian ignimbrites" and "Plinian ignimbrites" depending on the style of the eruption they are associated with. Larger ignimbrites that originated from caldera-forming eruptions along ring-fault fissure vents should be regarded as related to a separate eruption style - with respect to the common Hawaiian-Plinian trend -, where the effect of increased mass flow rate due to ring-fissure vents is dominant and controls the dynamics of the resulting collapsing fountains and pyroclastic flows, irrespective of the kind of eruption style that preceded the onset of the caldera collapse. These are named "caldera-forming ignimbrites" and are further subdivided into small, intermediate, large and super, based on their increasing erupted volume.

1. Introduction

Current classification and nomenclature of explosive eruption styles is based on monitored parameters or deposit characteristics, mostly related to eruptions that produce fallout deposits. Well established eruption styles from Hawaiian to Plinian reflect an increase in magnitude and intensity of the related eruptions although they can only be related to the specific phases or styles that form the fall deposits (lava fountains to buoyant plumes) (Walker, 1973; Cas and Wright, 1987; Pyle, 2015; Bonadonna and Costa, 2013; Bonadonna et al., 2016). A similar approach for deposits resulting from phases of eruptions where pyroclastic columns collapse, either partially or totally, and based on deposit characteristics, has never been proposed. This deficiency has made it difficult to relate deposits of collapsing pyroclastic columns, especially in the rock record, to specific eruption styles (with the notable exception of intra-plinian ignimbrites, i.e. ignimbrites embedded within Plinian fall deposits formed during the same eruption). The collapse of explosive eruption columns produces ground-hugging density currents

of hot mixtures of pyroclasts and gas, known as pyroclastic flows, pyroclastic density currents or just pyroclastic currents (e.g. Sparks et al., 1978; Cas and Wright, 1987; Branney and Kokelaar, 2002; Sulpizio et al., 2014; Palladino, 2017). As all these terms are still in use and are poorly differentiated from each other, they will be used interchangeably as synonyms in this paper. The associated deposits consist dominantly of poorly sorted juvenile ash and pumice (or scoria) known and herein referred to as ignimbrites.

Since the early works by Smith (1960a, 1960b), Fisher (1966) and Sparks et al. (1973), the term "ignimbrite" has been used mostly to describe welded tuffs, ash-dominated tuffs, and felsic pumice-and-ash flow deposits. "Ignimbrite" is defined here as: the rock or deposit formed from pumice and ash- through to scoria and ash-rich pyroclastic density currents, irrespective of their composition (ranging from rhyolite to basaltic), crystal content (from aphyric to larger than 50% by volume), volume (from less than millions of m^3 to several thousands of km^3), areal extent (from the order of 10^{-3} to 10^4 km^2), thickness (from less than 1 m to thousands of metres), relationship to paleotopography (from topography filling to topography draping, to topography burying), and temperature of emplacement (from above the glass transition temperature to close to ambient temperature) (Figs. 1 and 2). The common factors are similar flow and depositional mechanisms, as well their origin from eruption column or fountain collapse that generates a pyroclastic current.

The lithofacies associations of ignimbrites are usually, but not uniquely, dominated by massive deposits which may, and usually do, grade laterally and vertically to more internally organized structures (Fig. 2), including grading and/or alignment of components (juvenile and lithic clasts, as well as crystals), and more or less defined stratification, from parallel to cross-stratified.

The broad definition of the term ignimbrite adopted in this paper conforms with previous authoritative literature on pyroclastic flow deposits (e.g. Sparks et al., 1973; Cas and Wright, 1987; Branney and Kokelaar, 2002; Sulpizio et al., 2014 and references therein). Such deposits are distinct from block-and-ash flow deposits formed by the gravitational collapse of lava domes and deposits from laterally directed blasts, such as those derived from phreatomagmatic base surges and lateral sector collapses of volcanoes (e.g. the May 18, 1980 Mt. St Helens eruptions), even though the findings described in this paper may well apply also to these other kinds of deposits.

In this paper we propose an approach to classify ignimbrites, as we believe that the lack of a structured classification scheme has largely limited the development and the rigorous application of important descriptors of ignimbrites, such as their thickness decay patterns, areal extent and volume, in the way that the scientific community does for fallout deposits, starting with Walker's (1973) classification, with later updates (Pyle, 2015; Fierstein and Hildreth, 1992; Bonadonna et al., 2016). We propose and discuss large scale, first order field observables as descriptors that can be used as the basis for a classification scheme for ignimbrites, by following an approach to classification similar to that proposed by Walker (1973) for fallout deposits. The main intent of this paper is to stimulate discussion around this topic and to prompt a reappraisal of studies where first order field descriptors for ignimbrites, such as thickness and area of extent, are rigorously defined and measured. Such a scheme will then serve as a focus for developing a better understanding of the eruption dynamics and transport and depositional processes, as was the case following the release of the pyroclastic fallout deposit classification scheme by Walker (1973).
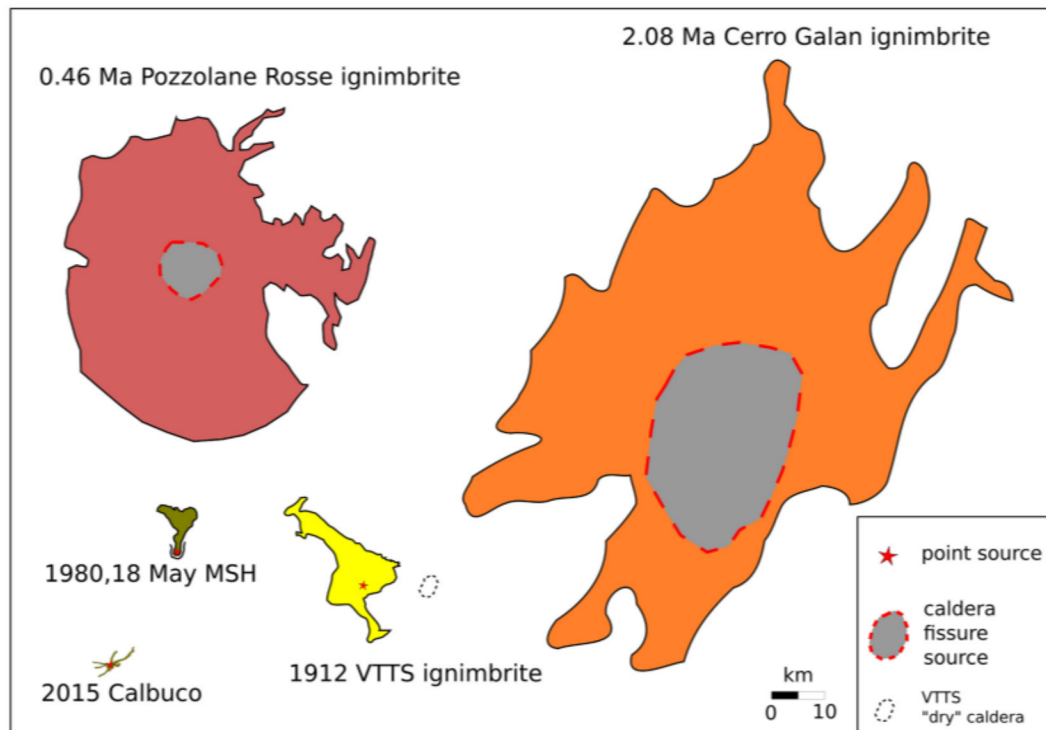

Fig. 1. Visual comparison of the huge variations in ignimbrite dispersals. At the lower end the small volume, valley pond ignimbrites produced by the partial collapse of a sub-Plinian column at Calbuco (Chile) in 2015 (Castruccio et al., 2016); the 0.12 km^3 valley confined pyroclastic flow deposits of the May 18, 1980 Mt. St Helens Plinian eruption, which followed the lateral sector collapse of the edifice; the 11 km^3, valley confined 1912 VTTS (Valley of Ten Thousands Smokes) ignimbrite is made of 9 packages originating from the collapse of a simultaneously buoyant Plinian column issued from a single vent, while a caldera formed 10 km away from vent (Hildreth and Fierstein, 2012); the 0.46 Ma, mafic Pozzolane Rosse axysimmetric ignimbrite formed during the collapse of the 8 km × 8 km Colli Albani caldera emplacing 59 km^3 of outflow ignimbrite, partly surmounted on and partly blocked by high mountain reliefs to the west (Giordano and Dobran, 1994)(Smith et al., 2020); the 2.08 Ma Cerro Galan ignimbrite formed during the 35 km × 25 km collapse of the caldera which emplaced 324 km^3 of partly welded outflow ignimbrite (Cas et al., 2011).
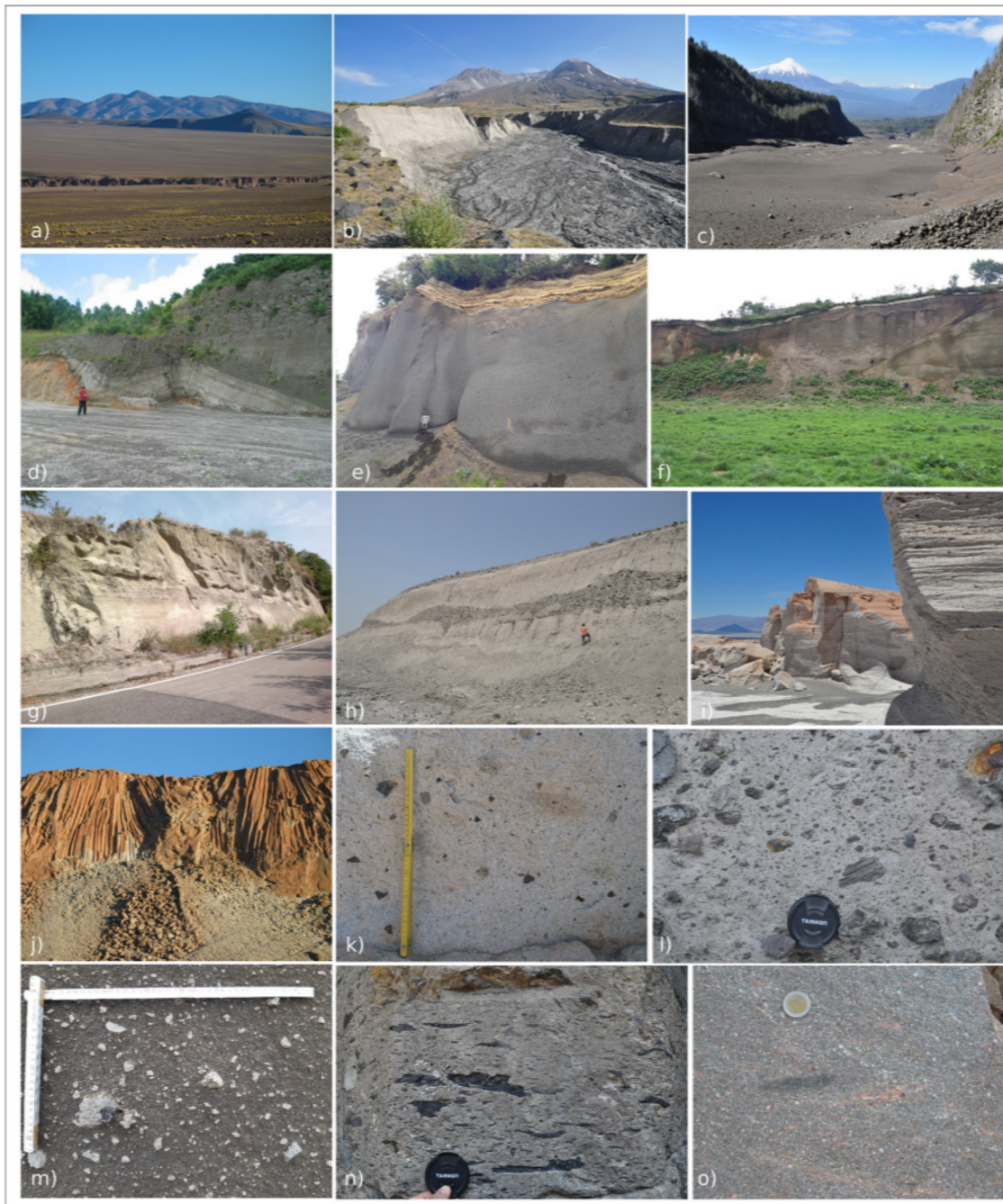
Fig. 2. Aspects of ignimbrites: a) topography burying ignimbrite shield formed by the 2.08 Ma, caldera forming, rhyodacitic Cerro Galan ignimbrite (Argentina); b) white cliffs cut in Pumice plain, made of dacitic ignimbrites of the 1980 Mt. St Helens Plinian eruptions (truncated edifice in the background; USA); c) valley filling, small volume ignimbrite of the 2015 subplinian Calbuco eruption (Chile); d) 4.6 ka Fogo A dark ignimbrite covering the white, topography mantling Plinian fall deposits (Azores); e) massive facies of the basaltic 12.4 ka, Caracautin ignimbrite (Chile); f) Shokotsu ignimbrite filling a paleovalley in the Kuttara caldera deposits (Japan); g) diffusely stratified facies of the White Trachytic Tuff Galluccio (Italy); h) lithic breccia lenses between ignimbrite depositional units of the 1980 Mt. St Helens Plinian eruption; i) diffusely stratified facies of the Quaternary Campo de la Piedra Pomez ignimbrite (Argentina); j) columnar jointing in unwelded, vapour-phase lithified Cerro Galan ignimbrite; k) typical massive lapilli tuff facies of the rhyodacitic, crystal rich Cerro Galan ignimbrite; l) typical massive lapilli tuff facies of the trachytic-phonolitic, crystal poor Campanian ignimbrite (Italy); m) typical massive facies of the basaltic, crystal poor Caracautin ignimbrite; n) welded facies (Piperno) of the Campanian ignimbrite; o) strongly welded, eutaxitic facies of the rhyolitic crystal rich Ora ignimbrite (Italy).

2. Review of pyroclastic density current deposits and processes

Pyroclastic deposits which are characteristically recognizable by their common poor sorting, fine ash matrix-supported texture, filling to draping attitude to topography and evidence for hot emplacement (Fig. 2) are associated with ground-hugging pyroclastic density currents. They have usually been characterised by their componentry, grain size and poor sorting. Common nomenclature includes pumice-and-ash (felsic-intermediate) flow deposits, scoria-and-ash (mafic) flow deposits, block-and-ash flow deposits, base surge deposits (Cas and Wright, 1987). In some instances, the association with a specific type of volcanic event has allowed a genetic interpretation to be applied to the deposits, such as for block-and-ash flow deposits, which are commonly related to gravitational and relatively weak explosive collapses of lava domes (e.g.

Cas and Wright, 1987; Freundt et al., 2000; Brown and Andrews, 2015), or as in the case of phreatomagmatic base-surge deposits and lateral blast deposits (Valentine and Fisher, 2000). However, the largest deposits preserved on Earth associated with ground-hugging pyroclastic currents derive from the partial to total collapse of magmatic to phreatomagmatic explosive eruption columns (e.g. Cas and Wright, 1987; Suzuki et al., 2005; Trolese et al., 2019). These encompass huge variations in composition (rhyolite to basalt), volume (from $<10^0$ km^3 to $>10^3$ km^3) and intensity (from $<10^7$ to $>10^{10}$ kg s^{-1})(Table 1), and are collectively known as pyroclastic density current (PDC) deposits, or ignimbrites (Sparks et al., 1973; Cas and Wright, 1987; Branney and Kokelaar, 2002; Brown and Andrews, 2015).

2.1. Flow types

(Wohletz and Sheridan, 1979) proposed a distinction between short-lived, time-transient, unsteady pulses or *pyroclastic surges* and related deposits, and maintained, steady, prolonged *pyroclastic flow* events (or ash-flows) and related deposits. Pyroclastic surges and flows have been seen as end members of the spectrum from *dilute* to *concentrated* density currents (Cas and Wright, 1987; Branney and Kokelaar, 2002). Developments in understanding the flow dynamics of pyroclastic density currents have progressively led to the recognition of a continuous spectrum in terms of their time- and space-dependent velocity and concentration profiles, emphasizing the shear coupling with the substrate at the lower flow boundary layer (e.g. Fisher, 1995; Branney and Kokelaar, 2002; Dufek et al., 2015; Zrelak et al., 2020).

Bursik and Woods (1996) modeled large volume pyroclastic flows as slow (10–100 m s^{-1}) and thick (1000–3000 m) *subcritical flows* and as fast (100–200 m s^{-1}) and thin (500–1000 m) *supercritical flows*. Their depth-averaged model predicted that the final runout is controlled mostly by the mass eruption rate, the air entrainment and the rate of sedimentation. Shimizu et al. (2019) used a two-layer model to account for the presence of a lower high-concentration zone and an upper dilute layer and their interaction. The model predicts that the final runout critically depends on the ratio between the depositional rate at the base of the basal dense current and the speed of particles settling from the upper dilute current into the lower dense current.

The dense basal undercurrent, where particle collisions, frictional effects and gas pore pressure play crucial roles in momentum transfer, can detach from the overlying dilute current and follow completely different paths in high topography relief areas, especially in currents that are small compared to topography roughness (e.g. Fisher, 1995; Fujii and Nakada, 1999; Druitt et al., 2002; Kelfoun et al., 2009; Esposti Ongaro et al., 2020).

Doronzo (2012) accounted for the energy-stratified nature of pyroclastic density currents (and/or parts thereof) by introducing the concept of a forced regime, where the energy is transported under the action of external forces, such as a sustained mass discharge rate (either at vent or along topography, e.g. along channels), and an inertial regime, where the energy is transported only by internal factors including turbulence and pore pressure. Sedimentation patterns are therefore proxies for different flow types (Andrews and Manga, 2012; Doronzo et al., 2016).

Vertical and lateral lithofacies variations within ignimbrites have been used to interpret their sedimentology in terms of local flow dynamics in relationship to topography, which has progressively become the main focus of field work and experiments on ignimbrites (e.g. Fisher, 1966; Sparks, 1976; Sparks et al., 1978; Wilson and Walker, 1985; Cas and Wright, 1987; Wilson et al., 1995; Valentine and Wohletz, 1989; Fisher et al., 1993; Branney and Kokelaar, 2002; Palladino and Valentine, 1995; Giordano, 1998; Fujii and Nakada, 1999; Giordano et al., 2002; Dufek and Bergantz, 2007; Cas et al., 2011; Sulpizio et al., 2014; Dufek et al., 2015; Brand et al., 2014, 2016; Roche et al., 2016; Breard and Lube, 2017; Palladino and Giordano, 2019; Báez et al., 2020; Smith et al., 2020; Lube et al., 2020). However, depositional lithofacies in

ignimbrites appear to be scale invariant, so their full spectrum from massive to stratified can be found in ignimbrites of any dimension and composition (Fig. 2; Branney and Kokelaar, 2002) and do not appear to be related to any specific eruption style.

Although the link between flow processes and deposit characteristics is still a matter of debate, a useful distinction is between: i) flows, or parts thereof, where density stratification allows the development of high concentration undercurrents which may (or not) detach from the overlying low concentration current and move independently to their final runout, especially where flows are small relative to topographic features (Fisher, 1995; Shimizu et al., 2019); these are typical of small volume flows channeled along rough and steep stratovolcano slopes (e. g. Fujii and Nakada, 1999; Giordano et al., 2002; Druitt et al., 2002; Pensa et al., 2015) or at distal ends of larger volume flows within high relief mountain areas (e.g. Baer et al., 1997; Ort et al., 2003; Silleni et al., 2020; Cas et al., 2011); ii) flows where density stratification and interaction with topography do not induce detachment of undercurrents and the maximum extent of the ignimbrite coincides with the maximum runout of the parent flow and the point of lift-off of the ash cloud (e.g. Bursik and Woods, 1996; Andrews and Manga, 2011; Shimizu et al., 2019); these are thought to be typical of ignimbrites associated with large volume flows, mostly caldera-related (and axisymmetric), thick with respect to topography and/or travelling on near-flat ground (with respect to flow) (e.g. Fisher et al., 1993; Wilson, 2001; Best et al., 2013; Giordano and Doronzo, 2017).

2.2. Vent geometries of collapsing eruptive columns

Since the classic works by Sparks (1976), Sparks et al. (1978) and Wilson et al. (1980), the conceptual model for the formation of ignimbrites is that of the partial to total collapse of Plinian columns originating from a cylindrical point-source vent (Fig. 3), as a result of either an increase in mass eruption rate (maybe related to widening of the vent) or decrease in gas fraction (cf. Suzuki et al., 2005; Trolese et al., 2019).

The common association of a basal Plinian fall deposit and an overlying ignimbrite sequence has motivated such a conceptual model (e.g. Cas and Wright, 1987; Branney and Kokelaar, 2002; Brown and Andrews, 2015), which has been implemented and developed in numerical modeling of collapsing plumes (e.g. Dobran et al., 1993; Suzuki et al., 2005; Esposti Ongaro et al., 2008; Trolese et al., 2017). Less frequently, ignimbrites are found interbedded with and/or laterally
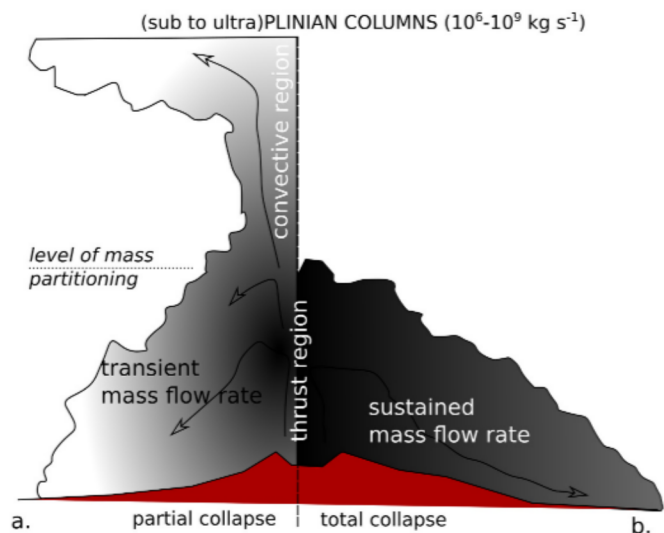
(sub to ultra)PLINIAN COLUMNS (10^6-10^9 kg s^{-1})

Fig. 3. Schematic diagrams of Plinian columns from point-sources showing: a) partial collapses that result in highly variable flow conditions; b) total collapses that transfer (almost) the whole mass flow rate into sustained pyroclastic flows.

equivalent to Plinian fall deposits and are interpreted as resulting from partial collapses of a sustained Plinian eruption column, or from alternating phases of column collapse and reactivation (e.g. Wilson, 2001; Wilson and Hildreth, 1997, 2003; Hildreth and Fierstein, 2012; Vona et al., 2020; Romano et al., 2020). Small volume pyroclastic flows and related deposits may also be associated with partial collapse of short-lived, impulsive Vulcanian columns (e.g. Nairn and Self, 1978; Druitt et al., 2002; Giordano and De Astis, 2021).

Pyroclastic currents originating during caldera collapses have instead long been envisaged as issuing from linear fissure vents along ring faults and/or other types of caldera faults (e.g. Smith and Bailey, 1968; Bacon, 1983; Rosi et al., 1983; Wilson and Hildreth, 1997; Vinkler et al., 2012). In this case the interpretation of the common, but certainly not ubiquitous, occurrence of a basal Plinian fall (+/− some early pyroclastic flow deposits) and subsequent widespread ignimbrites and associated co-ignimbrite breccias has been interpreted in terms of a two stage model, with an early, usually less voluminous phase of magma evacuation from a single point source vent producing a Plinian eruption style as a result of over-pressure in the magma reservoir, followed later by caldera collapse when the magma reservoir becomes under-pressured, allowing the opening of linear or ring fracture vents producing an immediately and fully collapsing, fissure fountain-like column (e.g. Bacon, 1983; Druitt and Sparks, 1984; Self et al., 1986; Geyer et al., 2006; Pinel and Jaupart, 2005; Geshi et al., 2014). The variation of eruption dynamics associated with the shift from single point-source vent to ring fault vent geometries has been discussed by Jessop et al. (2016) who concluded that linear vents favour collapse of the plume because of the reduction of air entrainment, and therefore explaining the usual overwhelming proportion of ignimbrites to fall deposits associated with catastrophic caldera collapses. Similar conclusions were reached by numerical modeling of the 161 ka Kos ignimbrite by Dufek and Bergantz (2007), who best-fitted the vent area at $>10^6$–10^7 m^2, much larger than single point explosive craters. Supporting this interpretation, some caldera-related ignimbrites totally lack a basal fallout deposits, suggesting that they did not form from collapse of an initially fully buoyant Plinian eruptive columns but from immediate collapse of fissure fed pyroclastic fountains (e.g. de Silva et al., 2006; Cas et al., 2011; Willcock et al., 2013; Palladino and Valentine, 1995).

2.3. Ignimbrite types and elements for their classification

The grading of eruptions by erupted volume and/or mass is the basis for the widely used Volcanic Explosivity Index (VEI, Newhall and Self, 1982) and Magnitude scale (Pyle, 2015). The VEI scheme does not distinguish among the origins of deposit types (e.g. effusive vs explosive, fall vs pyroclastic current), but by grading volumes by order of magnitude, it qualitatively distinguishes eruptions as "gentle" at <VEI1 ($<10^{-3}$ km^3), "explosive" at $2 < $ VEI $ < 4$ (10^{-3} - 10^{-1} km^3) and "cataclysmic, paroxysmal, colossal" at VEI > 4 (10^{-1} - 10^3 km^3). The VEI scale, as much as the Magnitude scale which grades the erupted mass, was clearly not devised to specifically classify ignimbrites. However, in explosive eruptions above VEI5, the proportion of ignimbrites in the total erupted products becomes increasingly overwhelming, so that ignimbrites are qualitatively distinguished based on their volume. Although not well characterised, common adjectives have been used to distinguish "small" (usually <1 km^3), "intermediate" (usually <10 km^3) and "large volume ignimbrites" (usually >10 km^3), the latter often qualified by further loosely defined descriptors at increasing volumes such as "very large" or "extremely large", when related to super-eruptions (usually >1000 km^3; Rampino, 2002). Lacking a specific eruption style to define large scale eruptions, Newhall and Self (1982) extended the Plinian eruption style to all eruptions above VEI4. This extension has later not been explicitly criticized or rediscussed, so in this way the Plinian eruption style has been implicitly extended to caldera forming eruptions and their products, which are dominantly ignimbrites. For this reason, even if the shift from single point vent to caldera

ring fractures has long been identified as the main process which favours the collapse of the eruption column, this process has somewhat remained embedded within the family of the Plinian eruption style, and so do the related ignimbrites, irrespective of their volume, dispersal and whether or not collapse of an initially buoyant Plinian eruption column was involved.

An early attempt to classify ignimbrites based on large scale field observables was proposed by Walker (1983) who described two main spectra of ignimbrite types: i) the low to high aspect ratio spectrum, and ii) the low to high grade welding spectrum. The low to high aspect ratio ignimbrites, so called LARI and HARI, were defined in terms of the ratio H/L, i.e. their average thickness, H, versus the diameter of a circle with an area equivalent to their dispersal area, L. HARI and LARI were defined by aspect ratio value ranges of 10^{-2}–10^{-3} and 10^{-4}–10^{-5} respectively. These end member values have been thought to reflect the way parent flows laterally transport (both along flow and across topography) their load of pyroclastic material, with HARI associated with low energy, rapidly sedimenting pyroclastic flows, whereas LARI represent highly mobile pyroclastic flows (Walker, 1983; Wilson and Walker, 1985; Cas and Wright, 1987). Bursik and Woods (1996; their fig. 12a) proposed a direct relationship between aspect ratio and total mass of the ignimbrites, i.e. at increasing mass erupted the aspect ratio increases, although the existence of such a relationship was later questioned by Freundt et al. (Freundt et al., 2000, their Fig. 2). Dufek (Dufek, 2016, Fig. 5) proposed that the increase of runout distance at increasing ignimbrite volume could be used as a proxy for mass eruption rate by comparing numerical models of Bursik and Woods (1996) and Dade and Huppert (1996).

Many detailed stratigraphic studies of ignimbrites have shown that some previously studied ignimbrites that were originally regarded as single ignimbrite units in fact consist of multiple, stacked depositional units, as well as reflecting the role of topography on deposition, making it difficult to relate unique values of thickness and areal extent (runout) to individual flow units (e.g. De Rita et al., 1998; Wilson, 2001; Wilson and Hildreth, 1997; Wilson and Hildreth, 2003; Báez et al., 2020). In time, HARI and LARI have consequently become loosely used and defined, mostly to distinguish topography filling and topography draping ignimbrite units respectively. In addition, especially for large volume ignimbrites, low aspect ratios ($<10^{-4}$) may not correspond to the expected topography draping, high energy flows, as in the case of the Cerro Galan ignimbrite (Cas et al., 2011). Giordano and Doronzo (2017) reappraised the concept of aspect ratio by suggesting, for individual depositional units, that the ratio at each locality between the local thickness and the distance along flow relative to maximum runout (therein introducing a topological aspect ratio ARt) is a proxy for the competition between deposition and transport integrated over the total duration of the pyroclastic current. The spatial gradient $\Delta ARt/\Delta x$ distinguishes forced regimes, for which the lateral thinning rates are mild, from inertial regimes that are illustrated by rapid lateral thinning rates. Palladino and Giordano (2019) have further explored the potential of the lateral variation rates of the maximum lithic and pumice clast sizes, in recognizing fundamental differences between end-member ignimbrites associated with purely inertial regimes and forced regimes respectively.

From the isopach map of the 22.5 ka Oruanui ignimbrite, Wilson (1991) noticed the existence of a linear relationship between the logarithm of thickness and cumulative area and volume enclosed by specific isopach contours. The author noticed also that this linearity could be a fortuitous consequence of the complex topographic control over the Oruanui ignimbrite dispersal pattern and recommended the need for more examples to be able to propose a possible generalized relationship. Later work by Wilson (2001) described the Oruanui ignimbrite as consisting of up to 10 depositional units separated by hiatuses and contemporaneous Plinian fallout deposits, accompanied by vent migration. However, according to the volume estimates by the same author, roughly two thirds of the total volume can be ascribed to the

final unit 10 ignimbrite, for which the calculated approximate distance from virtual source of 40–50 km covers the extent of the isopach map from which the log thickness versus area plot was retrieved. Based on these considerations the linearity observed by Wilson (1991) is not affected very much by the internal complications of the Oruanui stratigraphy. More recently, Silleni et al. (2020) extended Wilson's analysis to the Campanian ignimbrite and some other ignimbrites and found that the relationship between log-thickness and isopach area can be considered a feature of ignimbrites irrespective of paleotopography, although showing different decay rates.

Local occurrences of sedimentary structures and entrainment of accidental clasts have been used to constrain velocity and concentration of the basal parts of the flow in view of understanding the flow properties at the time of deposition (Pittari et al., 2006, Cas et al., 2011; Roche et al., 2016; Breard et al., 2018; Pollock et al., 2019; Smith et al., 2020) and are important features to be further explored in terms of differentiating flow types.

Walker (1983) proposed that the low to high grade welding spectrum of ignimbrites reflects the range of pyroclast temperatures and viscosities at the time of deposition (Quane and Russell, 2005) and Trolese et al., 2019) proposed that at increasing ignimbrite volumes the temperature of emplacement of pyroclastic flows also increases as a result of increased mass flow rates and lower levels of air entrainment (cf. Bursik and Woods, 1996; Jessop et al., 2016).

All the cited works identify the final geometry (aspect ratio, runout, thickness variations, grain-size patterns), volume, mass, and temperature of emplacement of ignimbrites as first order proxies for the eruption, transport and depositional processes associated with ignimbrites. In particular, the aspect ratio and the runout have been related to mass flow rates (e.g. Bursik and Woods, 1996; Shimizu et al., 2019), as well as volume (Dufek, 2016). However, none of these works have further explored these descriptors as a basis for classifying ignimbrites and their eruptions.

3. Field descriptors for a classification scheme of ignimbrites

3.1. Approach and limitations

Attempting a classification of ignimbrites is not an easy task. Following Walker's (1973) strategy for classifying fallout deposits, a meaningful classification should be based firstly on observables that can be relatively easy to retrieve from deposits of modern and ancient successions. The second fundamental is that these observable deposit characteristics are proxies that describe and link processes associated with eruption and pyroclastic current dynamics. Common field descriptors of ignimbrites at the outcrop scale are: thickness, lithofacies (including depositional structures and textures, composition, degree of welding and juvenile clast types), maximum clast size (juvenile and lithics), and crystal content (Cas and Wright, 1987). At the scale of the entire ignimbrite, variations are usually synthesized in terms of isopach maps (e.g. Best et al., 2013; Silleni et al., 2020), isopleth maps (e.g. Sparks, 1975; Milner et al., 2003), and welding degree/rank maps (e.g. Streck and Grunder, 1995; Lesti et al., 2011). These are also used to retrieve the maximum areal extent (used to infer the maximum runout of the parent flow), the maximum elevations overpassed, the aspect ratio and the bulk volume of ignimbrites. Each of the above listed descriptors are affected by varying degrees of uncertainty and errors in their determination, which are not always (in fact rarely) clearly identified in the literature that uses such descriptors (see discussions in Mason et al., 2004; Crosweller et al., 2012; Brown and Andrews, 2015; Silleni et al., 2020). For example, there are huge variations in the way the areal extent and bulk volumes of ignimbrites have been calculated (e.g. Wilson, 1991; Lipman, 1997; Mason et al., 2004; Geyer and Marti, 2008; Giordano and The CARG Team, 2010; Folkes et al., 2011; Crosweller et al., 2012; Best et al., 2013; Silleni et al., 2020). Furthermore, some ignimbrites are deposited with no time breaks and form a single cooling unit

(Smith, 1960b), although internally lithofacies may or may not define multiple depositional units according to variations in eruption dynamics and interaction with topography (e.g. Cerro Galan ignimbrite; Cas et al., 2011; Pozzolane Rosse ignimbrite; Giordano and Doronzo, 2017), whereas other ignimbrites include more than one cooling unit suggesting the occurrence of time breaks in deposition (e.g. Smith, 1960b; Wilson and Hildreth, 2003). In addition, the older the analysed unit, the larger is the extent of both areal and linear erosion which may affect the reliability of the reconstruction of the maximum area covered, hence the pyroclastic flow runout, and the total volume (Wilson, 1991). These uncertainty factors are much more relevant for volcanic islands and coastal volcanoes than for mainland deposits.

Nonetheless, provided all limitations and uncertainties are acknowledged, there is certainly a wealth of information in the existing literature that can be extracted. In Table S1 (Supplementary material) we summarize some of the field descriptors for 92 ignimbrites that are sufficiently well described in the literature to be considered comprehensive sources of data. These encompass a full range of volumes from small to large and are limited to outflow ignimbrites described as single cooling units. These are defined herein as emplaced without evidence for significant time breaks (e.g. presence within the ignimbrite sequence of paleosoils, fluvial erosion, deposition of reworked deposits, fallout deposits, evidence of differential cooling). Some well described units (e. g. Villa Senni Formation, Bishop Tuff, Oruanui ignimbrite, Valley of Ten Thousand Smokes ignimbrite) are sequences of multiple units. In these cases, Table S1 reports data for the most voluminous single cooling unit, unless otherwise indicated. We also point out that we limit our analysis to outflow ignimbrites, so we do not include intra-caldera fills in our list. 41 case studies are pre-Quaternary, the oldest being >38 Ma, while 13 are Holocene in age.

In order to be included in our dataset of Table S1 (Supplementary material), bulk volume, area and other values must have met at least one or more of the data quality indicators listed in Crosweller et al. (2012): i) isopach map (including its outer extent) based on >10 measurements; ii) description of calculation methods; iii) calculation of error and uncertainties.

Uncertainties on bulk volumes have been indicated where they are available in the original literature. For the rest of the dataset, we assume the uncertainties assessed by (Brown et al., 2014) on the comprehensive Large Magnitude Explosive Volcanic Eruptions (LaMEVE), estimated at below half an order of magnitude. It must be noted that we use bulk volumes and not Dense Rock Equivalent volumes, as we are interested in the geometry of the ignimbrites, not the source magma bodies. However, we caution the reader interested in Dense Rock Equivalent volumes about the variable densities of ignimbrites which vary from just above 1000 kg m^{-3} for unconsolidated deposits to near the dense rock equivalent density for highly welded ignimbrites.

The areal extent of ignimbrites is also affected by significant uncertainties, which become larger as we go back in the rock record and the effects of erosion increase. Streck and Grunder (1995) classified the reconstructed dispersal area of the Rattlesnake ignimbrite based on the degree of interpolation and extrapolation of real outcrops as "certain", "very likely", "likely" and "probable". The "probable" area was estimated at 40% of the total. Silleni et al. (2020) reconstructed a very detailed isopach map for the Campanian Ignimbrite (based on 335 measured outcrops and more than 300 bore hole stratigraphies) and calculated the dispersal area as that enclosed in the 0 isopach; however, as the ignimbrite in distal areas is only preserved as valley pond within high relief mountains, the area enclosed by interpolating the most distal outcrops increases by 45% and was considered reliable by the authors as erosion and/or non-deposition are considered responsible for the present lack of deposit along the steep and high mountain slopes. A similar value of 45% was calculated by Scott et al. (1996) for the area covered by the thin and discontinuous distal deposits respect to the total area of the pyroclastic flow deposits of the 1991 Pinatubo eruption. Such kinds of detailed assessment of the dispersal areas are rare in the literature.

However, based on the described examples we assume that the error on areal extent is below 50% and most likely underestimates the original extent, as erosion progresses (Wilson, 1991).

3.2. Main relationships identified: runout, area, volume and aspect ratio

Table S1 summarises data from 92 case studies, which range from very small (<<1 km³) valley confined intra-plinian ignimbrites to the largest ignimbrites on Earth, covering almost all sizes, compositions, welding rank and crystal contents. Outflow area and bulk volume are the two most common quantities that we found in the literature, although as mentioned earlier, there are only rare case studies with well-defined methods of calculation, errors and uncertainties (e.g. Mason et al., 2004; Folkes et al., 2011; Silleni et al., 2020). Outflow areas and bulk volumes can be used to calculate the average thickness and the equivalent radius, which is a proxy for the runout of the parent pyroclastic current. The equivalent diameter (i.e. the diameter of the circle with area equivalent to that of the ignimbrite areal extent) can be used to calculate the Aspect Ratio (AR) sensu Walker et al. (1980). As discussed in Wilson (1991), the preserved volume in the rock record is much less affected than the preserved area by erosion, so, in principle, aspect ratios may be over-estimated in ancient ignimbrites due to a less than actual evaluation of their original, maximum areal extent. However, the selected case studies in Table S1 include both recent and ancient ignimbrites and all are based on large field datasets, so that the figures reported for the outflow area already take into consideration issues about distal erosion.

In Fig. 4 we plot bulk volumes versus aspect ratios, a diagram that was presented originally as aspect ratio vs mass of the deposit, in Bursik and Woods (1996), who suggested a negative relationship, i.e. a decrease of the aspect ratio at increasing magnitude of the ignimbrite, but with just 8 data points. Later, Freundt et al. (2000) extended the dataset to 19 points and questioned the existence of any relationship between volume and aspect ratio. Fig. 4 plots our 92 points and confirms the lack of the correlation originally proposed by Bursik and Woods (1996), which is disappointing if we aim to use geometric parameters to distinguish ignimbrite types.

We now explore the approach by Dufek (2016), who showed a power-law relationships between volume and runout of the parent pyroclastic currents by comparing results of numerical models of Dade and Huppert (1996) and Bursik and Woods (1996) at different initial gas mass fractions, for ideal axisymmetric and flat topography conditions, which fitted values of volume and runout of 7 ignimbrite case studies:

Taupo, Ito, Koya, Rattlesnake, Bishop, Bandelier and Kos ignimbrites. In Fig. 5 we compare the numerical results of Dufek (2016) with bulk volumes and runout expressed as the equivalent diameter of the dispersal area of all 92 ignimbrites listed in Table S1 (Supplementary material). Out of the entire dataset, 80% of ignimbrites plot within predictions of numerical models at different initial gas mass fractions as proposed by Dufek (2016), and the overall dataset shows a good correlation on a power law fit ($R^2 = 0.87$). The confirmed correlation of erupted volume and runout is promising for classification purposes and is discussed in the next section.

In Fig. 6 we plot volume and dispersal area of the same ignimbrite dataset on a log-log diagram. We use the area of dispersal instead of runout, because it is a more commonly measurable value for mapped ignimbrites, which can in turn be used to calculate the equivalent runout as the radius of the circle of equivalent area; logically, the diagram shows a similar good correlation as equivalent radius (or runout) shown in Fig. 5 is simply derived from the equivalent area. The plot is also contoured for the extreme values of low aspect ratio (10^{-5}) and high aspect ratio (10^{-2}), which fit almost the entire dataset. Interestingly, the correlation line is perfectly parallel to the lines of equal aspect ratios showing that most of the analysed ignimbrites have aspect ratios comprised between 10^{-3} and 10^{-4}. The variability of aspect ratios indicates the spectrum from topography draping LAR ignimbrites, topography burying/building ignimbrites and topography filling HAR ignimbrites. The contours for different aspect ratios also broadly coincide with the numerical modeling of volume and runout by Dufek (2016) at varying initial gas content (cf. Fig. 5).

4. Discussion

4.1. Classification of ignimbrites

The results discussed in the previous section suggest that first order descriptors such as the areal extent, runout and deposit volume can discriminate first order differences among ignimbrites that are worth discussing as the basis for their classification.

The diagrams in Figs. 5 and 6, which relate volume, runout and dispersal area show quantities that are commonly described or retrievable for mapped ignimbrites and unique for each ignimbrite, within uncertainties and errors in their determinations as discussed above. The correlation of values and the spread across the diagrams are also important aspects for classification.

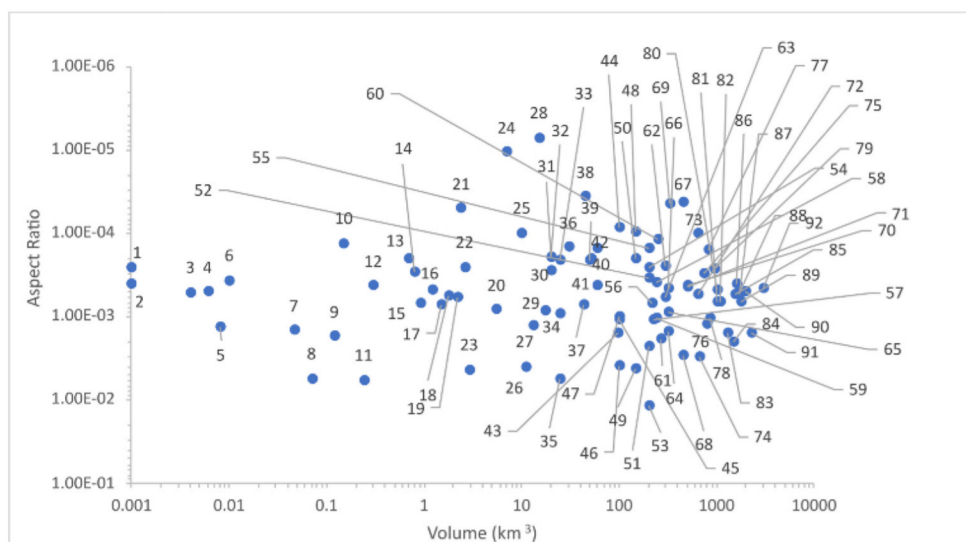Numerical modeling indicates that in axisymmetric conditions the

Fig. 4. Bulk volume versus aspect ratio plot of ignimbrites. Legend (see Table S1 in Supplementary material for all individual values).
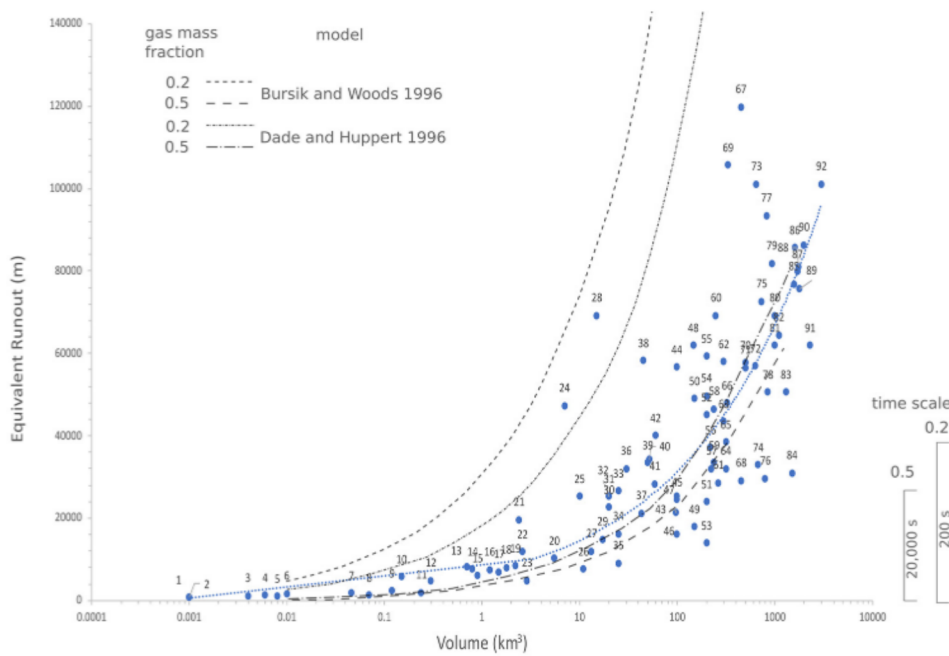
Fig. 5. Bulk volume versus runout taken as the equivalent diameter of the maximum area covered by plotted ignimbrites; dataset as in Fig. 4 (see Table S1 for individual values); curves of volume and runout from numerical modeling by Dufek (2016) are plotted for different initial gas fractions (0.2 and 0.5) and different numerical approaches (Bursik and Woods, 1996; Dade and Huppert, 1996). The dotted blue line depicts the best fit correlation line ($R^2 = 0.87$). (For interpretation of the references to colour in this figure legend, the reader is referred to the web version of this article.)
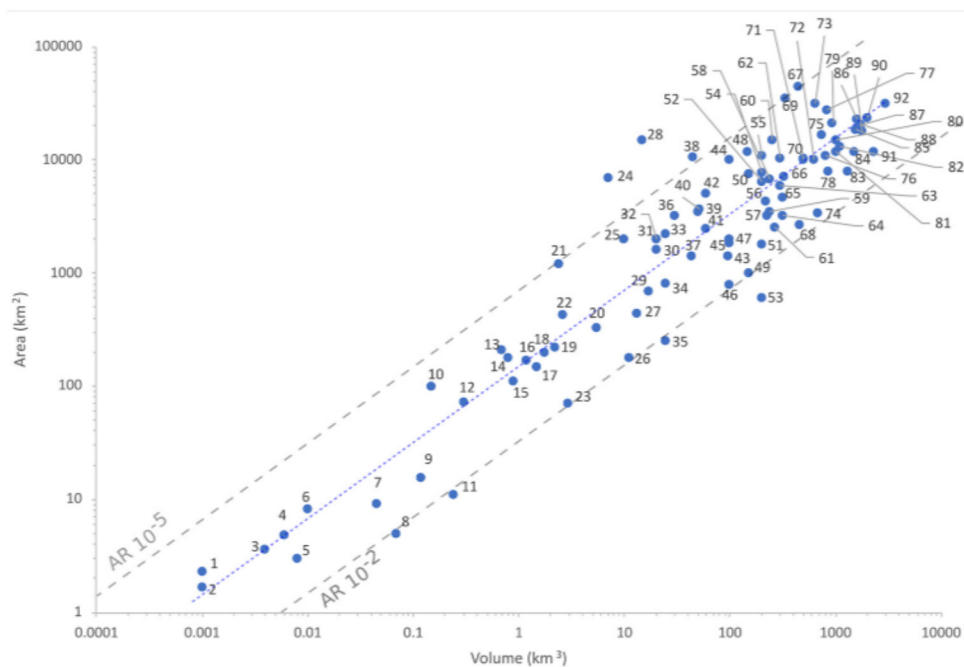

Fig. 6. Log-log diagram for deposit volume and dispersal area of ignimbrites; dataset as in Fig. 4 (see Table S1 for individual values). Dashed lines indicate Aspect Ratios (AR) and the extreme values of LARI (10^{-5}) and HARI (10^{-2}). The best fit line (blue dashed line; $R^2 = 0.88$) indicates that most common aspect ratios are comprised between 10^{-3} and 10^{-4} . (For interpretation of the references to colour in this figure legend, the reader is referred to the web version of this article.)

runout of ignimbrites' parent currents and, therefore, their dispersal area are linked to the mass flow rate feeding the pyroclastic current (e.g. Bursik and Woods, 1996; Dufek, 2016; Shimizu et al., 2019). We have 14 case studies in our dataset of Table S1 (Supplementary material) for which the mass flow rate is reasonably well constrained, and which show an excellent correlation with the equivalent runout calculated from our dataset (Fig. 7). This relationship indicates that dispersal area and equivalent runout of ignimbrites are field measurable which represent proxies for mass flow rates.

The final volume of the ignimbrite is instead related to the total mass emplaced as pyroclastic flows across the duration of the eruption, so that

for any given mass flow rate, the volume is a proxy for the eruption duration. In addition, for most of the large volume eruptions, ignimbrites form the largest part of the total erupted volume. By transforming the bulk volume in dense rock equivalent (DRE) volume and the latter into mass we can then measure the Magnitude (M) of the eruption according to M = $\log_{10}$ [DRE (m^3) * magma density (kg/ m^3)]-7, where DRE (m^3) = [bulk volume (m^3) * ignimbrite density (kg/ m^3)/ magma density (kg/ m^3)] (Pyle, 2015).

The relationship between Magnitude (total mass erupted) and Intensity (mass eruption rate) has been explored by Pyle (2015) and Brown and Andrews (2015), who showed that the two quantities are
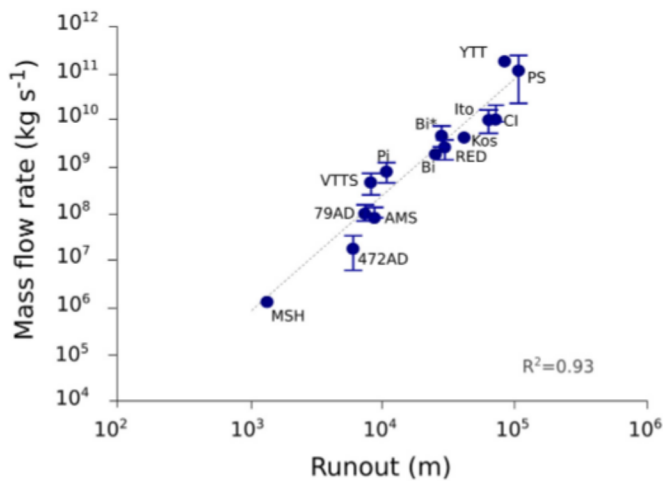
Fig. 7. Mass flow rate versus runout for 14 case studies (data in Table S1 of supplementary material). Legend: MSH – July 22, 1980, Mt. St Helens; 472 CE – Pollena eruption, Vesuvius; 79 CE – Pompei eruption, Vesuvius; VTTS – 1912 Valley of Ten Thousand Smokes, Novarupta; Pi – 1991 Pinatubo; Bi – Bishop Tuff compound; Bi* - Bishop Tuff, Ig1; RED – Pozzolane Rosse ignimbrite; Kos – Kos ignimbrote; Ito – Ito ignimbrite; CI; Campanian ignimbrite; PS – Peach Spring Tuff; YTT – Young Toba Tuff. Runout is expressed as the radius of the circular area equivalent to the dispersal area of the ignimbrite. The mass flux are data available in the literature and derive from geological constraints (e.g. Bi, VTTS, PS), observations (e.g. MSH, Pi, VTTS), or numerical modeling (e.g. 79 CE, 427 CE, RED, Kos, CI, Ito, YTT). (For interpretation of the references to colour in this figure legend, the reader is referred to the web version of this article.)

positively correlated and reflect the full spectrum of eruption styles from mild to highly explosive. This correlation confers a strong physical meaning to the volume and area/runout correlation observed in Fig. 6.

Based on the above discussion, we draw Fig. 8 as log volume vs log area of ignimbrites, setting the basis for our classification proposal. The diagram is equivalent to that of Walker (1973) for fall deposits in that it

shows two field measurable quantities that relate to the Magnitude and the Intensity of the event. The ignimbrite field is delimited by lines parallel to equal aspect ratios (cf. Fig. 6) and which enclose almost all 92 case studies of our dataset.

We subdivide the ignimbrite field at volume intervals of <1 km^3, 1–10 km^3, 10–100 km^3, 100–1000 km^3 and > 1000 km^3, corresponding to the established progression of VEI < 5 to VEI8 (Newhall and Self, 1982; Pyle, 2015). The boundaries between fields are not sharp in Fig. 8, but encompass the uncertainty on volume estimates, which, as discussed earlier in the text, has been evaluated at less than half of an order of magnitude by (Brown et al., 2014). The lower field (< 1 km^3) includes ignimbrites fed by partial to total column collapses from point source vents associated with eruptions of the Plinian family (sensu Walker, 1973). At the lower end, we can also include ignimbrites associated with Vulcanian eruptions (and in principle also block-and-ash flow deposits). In order to reduce the introduction of new nomenclature, our suggestion is to simply add to ignimbrites in this field the adjective of the related eruption style sensu Walker (1973). Therefore, in this field we name "Vulcanian ignimbrites" as those that form from column/fountain collapse during Vulcanian eruptions (e.g. Ngauruhoe 1975, Nairn and Self, 1978; Lube et al., 2007; Monterrat, 1997, Cole et al., 2002; Druitt et al., 2002; Stromboli 2019, Giordano and De Astis, 2021) and "Plinian ignimbrites" those associated with the partial to total collapse of Plinian columns originating from single point sources (the whole family from sub- to ultra-Plinian)(e.g. Mt. Vesuvius, 472 CE, Sulpizio et al., 2007, Vona et al., 2020; Mt. St Helens 1980, Rowley, 1981; Brand et al., 2016; Chaiten, 2008, Major et al., 2013; Calbuco 2015, Romero et al., 2016; Castruccio et al., 2016), as the occurrence of such ignimbrites does not require a change in the nomenclature of the overall eruption style. In this sense, the commonly described intra-plinian ignimbrites (i.e. those that occur from partial collapse of a more or less stable column and are found interbedded within a Plinian fall deposit sequence) are part of the larger family of Plinian ignimbrites (e.g. 4.6 ka Fogo A black and pink ignimbrites, Pensa et al., 2015; 4.5 ka Agnano Monte Spina units A and B, Romano et al., 2020).

We propose that the 1–10 km^3, 10–100 km^3 and 100–1000 km^3 and > 1000 km^3 fields in Fig. 8 distinguish small, intermediate, large and
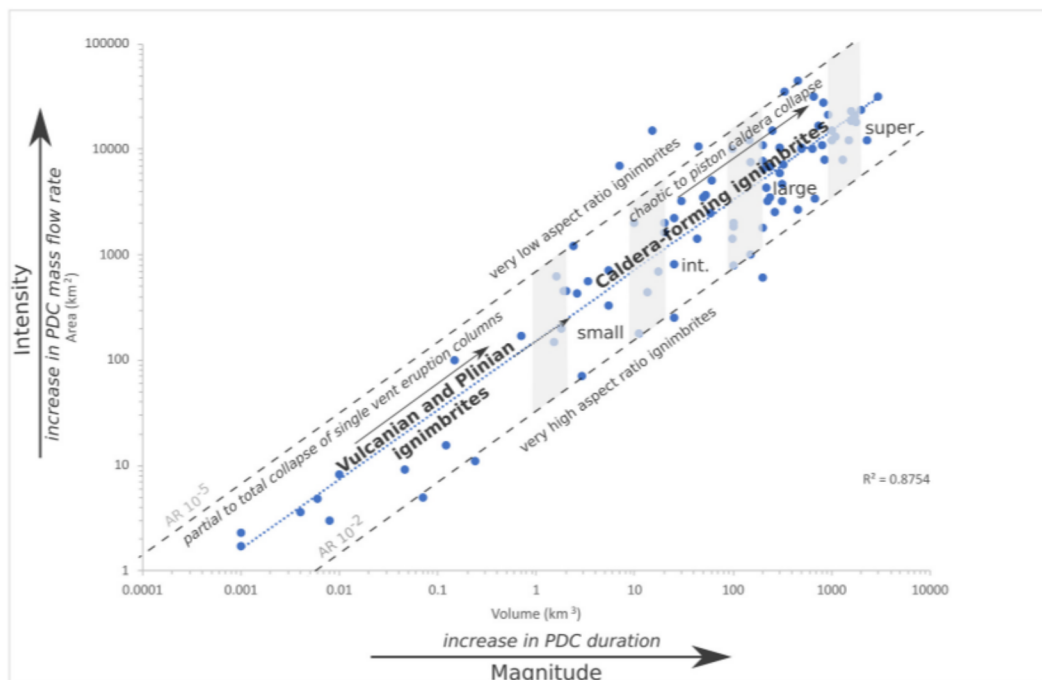

Fig. 8. Classification diagram for ignimbrites. See text for explanation.

super caldera-forming ignimbrites (cf Volcanic Explosivity Index of Newhall and Self, 1982, and the definition of super-eruptions; Miller and Wark, 2008; Wilson, 2008).

In the 1–10 km^3 field, most ignimbrites are caldera-forming (Table S1) but certainly not all of them, as few Plinian ignimbrites from single point sources may reach volumes larger than 1 km^3. For example, a remarkable outlier of point source vent-derived ignimbrite family is the Valley of Ten Thousand Smokes ignimbrite (VTTS), which is 11 km^3 as total volume, and certainly caldera related but oddly erupted across 16 h from an eccentric single point-source vent (Novarupta locality), while caldera collapse occurred some 10 km away (Fig. 1). So, in spite of its volume and association with a caldera collapse, it should be included in the Plinian ignimbrites family. In agreement with this interpretation, the VTTS was emplaced in 9 pulses, contemporaneously with a sustained pumice fallout, indicating that column collapses occurred repeatedly while the feeding, single point-source-derived Plinian column was persistently in existence (Hildreth and Fierstein, 2012). Based on this Fig. 8 shows a dotted arrow which extends large Plinian ignimbrites into the 1–10 km^3 field.

Within the family of the caldera-forming ignimbrites, the distinction in terms of volume is interesting because it corresponds to an increase in runout and dispersal area (Shimizu et al., 2019) which in turn reflects the progressive increase in mass flow rate feeding the PDC at increasing total length of the erupting ring-faults. Therefore, this distinction refers to changes in eruption dynamics associated with variable caldera collapse mechanisms (e.g. Lipman, 1997; Cole et al., 2005; Branney and Acocella, 2015). Results from analogue and numerical modeling of caldera formation show a major distinction between chaotic and coherent collapses (Roche et al., 2000; Kennedy et al., 2004; Geyer et al., 2006). In particular, Roche and Druitt (2001) and Geyer et al. (2006) found that thin and wide roofs associated with relatively shallow and wide magma reservoirs promote the coherent collapse of a piston block across a well-defined ring fracture, whereas thick and narrow roofs associated with relatively deep and small reservoirs promote chaotic collapses that involve the progressive upward excavation of the roof until complex sets of ring faults eventually reach the surface (Fig. 9). Piston collapses are therefore more likely associated with evacuation of large volume reservoirs (Cashman and Giordano, 2014). Gregg et al. (2012) placed the boundary between chaotic and piston collapses at caldera areas around 100 km^2. Apart from the actual volume value for setting this boundary, what is interesting here is that, given the well-established direct relationship between ignimbrite volumes and caldera areas (Smith, 1979), the change in caldera collapse dynamics occurs with increasing erupted volume, which for these large eruptions is measured by the ignimbrite volume. In turn, the mass flow rate feeding the pyroclastic flows can only increase with increasing length of erupting ring fissure vents, hence with increasing area of the caldera. We interpret that the transition from chaotic to piston collapses controls the eruption style, which may be quite variable in chaotic collapses where the progressive excavation of the roof generates many sets of faults and conditions for a variety of point source vents and eruption styles (Fig. 9a), compared to much more steady, sustained "boiling-over" fountains at extreme mass flow rates from extensive ring fault vents in piston collapses (Fig. 9b).

We therefore suggest that at the lower end of the caldera-forming ignimbrites (i.e. <100 km^3), where chaotic caldera collapses most likely occur, there are more chances to produce a variety of eruption dynamics resulting in wide-ranging values of ignimbrite geometries, in contrast with more restricted eruptive conditions at increasing volumes (1000 km^3) leading to piston collapses, where mass flow rates can be
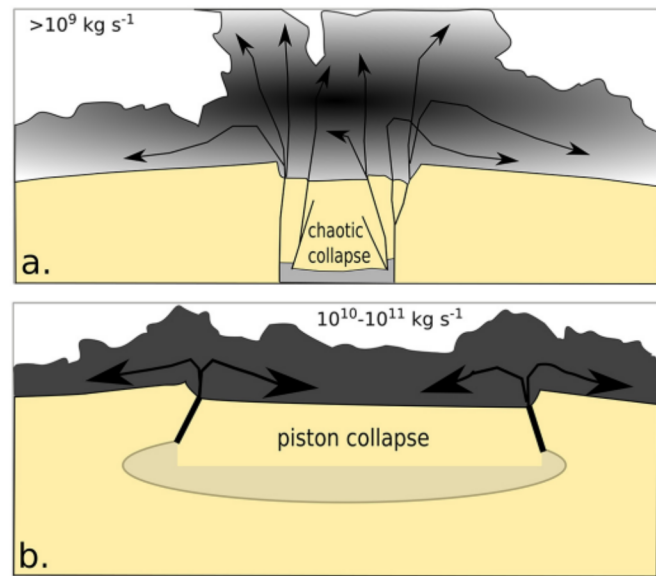

Fig. 9. Different caldera collapse mechanisms may explain the higher mass flow rates needed for large volume ignimbrites related to piston collapses b), as opposed to much more variable conditions in eruption related to smaller chaotic caldera collapses a). Arrows and caldera faults thickness are qualitatively proportional to mass flow rate as well as the grey scale in the pyroclastic flows.

huge and sustained, resulting in a more limited range of ignimbrite geometries (Fig. 6; Table 1).

Some well described examples of caldera-forming ignimbrites corroborate the complex progression of caldera ring-faults, suggestive of chaotic caldera collapse. This style of caldera collapse generates shifts of point source vents from which an alternation of sustained and collapsing column phases may occur, until climactic caldera collapse (e.g. Oruanui ignimbrite, Wilson, 2001; Bishop Tuff, (Hildreth and Mahood, 1986) Wilson and Hildreth, 2003; 184 ka Lower Pumice, Santorini, (Simmons et al., 2016); 151 ka Sutri Formation, (Bear et al., 2009); 6845 y.B.P. Crater Lake, (Druitt and Bacon, 1986)). In this sense, a caldera-forming ignimbrite sequence may be constituted by different types of ignimbrites and a progression of caldera collapse styles (e.g. Branney and Acocella, 2015). This appears to be the case of the Oruanui ignimbrite (Wilson, 2001), where the early small volume PDC units (units 1, 2, 4, 5, all <1 km^3 in Wilson, 2001) could be classified as Plinian ignimbrites associated with repeated collapses of Plinian columns. These were followed by small to intermediate volume caldera-forming ignimbrites (units 3, 6, 7, 8, 9 each in the order of 10^1 km^3 in Wilson, 2001) related to the beginning of caldera ring-fault step-like unzipping, and eventually to the eruption of the final large volume ignimbrite (unit 10 in the order of 10^2 km^3 in Wilson, 2001) related to the final wholesale caldera collapse. Such progression, though step-like, implies a progressive increase in mass flow rate. It must be noted that Wilson (2001) described some of the small to intermediate volume caldera-forming ignimbrites as much more extensive (up to 90 km from vent for unit 8) than the final large volume caldera-forming ignimbrite (up to 45 km from vent for unit 10, though not constrained at the distal end). However, such variability is well within the range shown in Figs. 5 and 6 and confirms that quite large variations in areal extent and aspect ratios are expected at the lower end of the caldera-forming ignimbrite family. Such variations are

usually not described for super caldera-forming ignimbrites ($>10^3$ km^3) (e.g. Chesner and Rose, 1991; Lindsay et al., 2001; Maughan et al., 2002; Willcock et al., 2013; Best et al., 2013). In agreement with this interpretation, recent work by Roche et al. (2016) suggests, based on field evidence, extreme mass flow rates up to 10^{10}–10^{11} kg s^{-1} for the Peach Spring Tuff (Fig. 7; cf. Table S1), which can be accomplished only by taking into account the sustained outpouring from extensive ring-faults (Costa et al., 2018). A similar conclusion was suggested for the large volume Cerro Galan ignimbrite (Cas et al., 2011) and for the Youngest Toba Tuff (Costa et al., 2014). These mass flow rates values are up to three orders of magnitude larger than those known for Plinian columns derived from point-source vents and for small to intermediate caldera-forming ignimbrites, such as the Campo de la Piedra Pomez eruption (Báez et al., 2015; Báez et al., 2020), Novarupta 1912 (Fierstein and Hildreth, 1992) and Vesuvius 79 CE (Sigurdsson et al., 1985; Cioni et al., 2008).

The very high mass fluxes associated with ring-fault caldera collapses (Jessop et al., 2016) and their progression from chaotic to piston style, may also explain other common features of intermediate and large caldera-forming ignimbrites: i) high temperature of emplacement and welding (see Trolese et al., 2019, their Fig. 1), and ii) a limited degree of internal stratigraphic complexity (e.g. Cas et al., 2011; Willcock et al., 2013; Roche et al., 2016; Silleni et al., 2020). These patterns could be interpreted in terms of forced convection dominated pyroclastic flows (Doronzo, 2012), where the forcing agent is the high mass flow rate which allows the internal flow pressure, promoting transport to be maintained over time and space, and at the same time the depositional rate (Giordano and Doronzo, 2017; Shimizu et al., 2019). Furthermore, at increasing mass flow rates within pyroclastic flows, air ingestion and cooling are largely prevented from accessing the basal high concentration part of the flows, favouring hot sedimentation (e.g. Andrews and Manga, 2012; Doronzo et al., 2016; Trolese et al., 2017, Trolese et al., 2019).

It is important to clarify that we do not imply that *all* calderas related to small to intermediate volume ignimbrites collapse with a chaotic mechanism, nor that their eruptive behavior should necessarily follow a complex pattern. Similarly, we do not imply that all calderas related to large and super caldera-forming ignimbrites collapse only with a simple piston mechanism. However, there clearly seem to be some general patterns which we have now highlighted.

We have demonstrated that volume and dispersal area/runout are field measurable properties of ignimbrites that reflect increasing magnitude and mass flow rate (intensity) of the related pyroclastic flows. In addition, increasing values of these parameters coincide with transitions in classic eruption styles, to which we propose to add the caldera-forming eruption style. This is a very distinct style from Plinian, as the fissural geometry of the vents during caldera collapse promotes continuous fountaining of the eruption columns, at increasing mass fluxes for progressively larger calderas.

In Table 1 we summarize some of the most important features that characterise the various eruptions styles in order to better appreciate how our proposal captures eruptive styles that currently have no specific nomenclature. In detail we propose that Walker's nomenclature can be applied to eruptions generating PDC deposits only when related PDCs are associated with collapses of eruptive columns derived from point source vents. Available data indicate that these kind of PDCs are associated with mass eruption rates between 10^6 and 10^9 kg s^{-1}, which cover the typical range of mass eruption rates for point-sourced Vulcanian to Plinian eruptions. By contrast ignimbrites associated with caldera-forming eruptions (or caldera-forming phases of an eruption sequence) should not be confused with collapses of single point-source vent eruption columns, as pyroclastic flows originating from ring-faults are sustained by much higher mass flow rates, up to 3–4 orders of magnitude larger (up to 10^7–10^8 m^3 s^{-1} in Roche et al., 2016 and 10^9–10^{11} kg s^{-1} in Costa et al., 2018; see also the fast time scales of deposition implied by modeling welding in Lavallée et al., 2015), that result in different

Table 1

Summary of the main characteristics of different eruption styles including the newly proposed caldera-forming style and the various ignimbrite types according to the nomenclature proposal of Fig. 4. Plume heights for caldera-forming eruptions are from Costa et al. (2018), who by numerical simulations propose that giant clouds from large volume ignimbrite-forming eruptions may reach as much as 80 km in height (*not verified). The other values are those most commonly reported although variations are discussed in the vast literature associated with each style (not reported here).

Eruption Style	Feeding	Intensity (kg s^{-1})	Vent geometry	Column type	Column height (km)	pdc	Ignimbrite type	Ignimbrite volume (km^3)	Composition
Strombolian s.s.	long term intermittent	$<10^4$	single point	jet	<0.5		N/A		mafic
Hawaiian	sustained (short lived)	$<10^6$	fissure/ single point	jet ± weak convective	< 5		N/A		mafic
Violent Strombolian	short term intermittent impulsive	$<10^6$	single point	weak convective	< 10		N/A		mafic-intermediate
Vulcanian		$<10^7$	single point	weak convective	< 15	possible	Vulcanian ignimbrites	$< 10^{-1}$	mafic-intermediate-felsic
subPlinian	sustained	10^6–10^7	single point	weak to strong convective	15–20	possible	Plinian ignimbrites	$\leq 10^{-1}$	mafic-intermediate-felsic
Plinian (and ultra-)	sustained	10^7–10^9	single point	strong convective	20–35 (50?)	frequent	Plinian ignimbrites	$\leq 10^0$ rarely up to 10^1	mafic-intermediate-felsic
Caldera-forming	sustained	10^9–10^{11}	segmented ring-faults (chaotic collapse)	collapsing fountain + co-ignimbritic	up to 80*	dominant	small to intermediate Caldera-forming ignimbrites	10^0–10^2	mafic-intermediate-felsic
			segmented to continuous ring-faults			dominant	large Caldera-forming ignimbrites	10^2–10^3	intermediate-felsic
			continuous ring-faults (piston collapse)			dominant	super Caldera-forming ignimbrites	$>10^3$	intermediate-felsic

collapse dynamics and PDC mobility (Jessop et al., 2016; Shimizu et al., 2019).

We underline here that the presence or not of a classic Plinian fall deposit at the base of caldera-forming ignimbrites is in our opinion not sufficient for the definition of the related eruption style (e.g. Palladino et al., 2010; Cas et al., 2011; de Silva and Gregg, 2014; Roche et al., 2016). In this sense, while the transition from a basal fall deposit into Plinian ignimbrites (e.g. the classic intra-plinian ignimbrites) can be justified by classic column collapse models (Wilson et al., 1980; Dobran et al., 1993; Suzuki et al., 2005; Trolese et al., 2019), caldera-forming ignimbrites, even where covering pumice fall deposits, should be modeled with ring-fault pyroclastic fountains with increasing total length. Such a conclusion is corroborated by recent numerical modeling of caldera-related super-eruption columns that appear to diverge from single point-source vent derived columns, supporting the transitions to specific dynamics associated with large mass flow rates (Costa et al., 2018).

5. Summary and conclusions

This paper reappraises the importance of first order geometric descriptors for ignimbrites for their comparison and for developing a better understanding of the spectrum of the related eruption and flow processes. By compiling and analyzing a dataset of morphological data for single cooling/depositional units of 92 outflow ignimbrites (Table S1 in Supplementary material), we propose a classification scheme based on the correlation of bulk volume and dispersal area (Fig. 6). The dispersal area (in turn related to runout) is controlled by the mass flow rate feeding the pyroclastic flow (Fig. 7), whereas final volume is controlled by the mass flow rate and the duration of the flow event. Volume and area are therefore proxies for magnitude and intensity respectively. These correlations are strongly grounded on current understanding of the physics of pyroclastic flows.

We propose to clearly distinguish ignimbrites deriving from collapses of eruption columns issuing from single, point source vents, from those derived from ring-faults during caldera collapses (Fig. 8). We relate the former to Walker's (1973) classification scheme of eruption styles (Hawaiian to Ultraplinian) and named herein "Vulcanian ignimbrites" and "Plinian ignimbrites", depending on their origin from the collapse (or partial collapse) of a Vulcanian or a Plinian (including sub- and ultraplinian) column. Ignimbrites derived from ring-fault fissure vents during caldera collapses are herein named "caldera-forming ignimbrites" and could be subdivided into a gradational spectrum of "small" (10^0–10^1 km^3), "intermediate" (10^1–10^2 km^3), "large" (10^2–10^3 km^3) and "super" ($> 10^3$ km^3). We stress that the term caldera-forming ignimbrites (as was the case for the terms Hawaiian, Strombolian, Plinian. Vulcanian at the time of Walker's classification) is already well established in the literature, but we have formalized it here in terms of volume-area, hence magnitude and intensity, as an additional eruption style with respect to those defined by Walker (1973). We also underline that once adopted, the proposed classification can be applied to ignimbrites in the rock record, where vent areas may not be in outcrop.

The progressive increase in mass flow rate associated with the transition from partial collapses to total collapses of eruption columns for single point-source derived ignimbrites and with the transition from chaotic to piston caldera collapses at increasing volumes for caldera-forming, ring-fault related ignimbrites may result in both the progressive increase in runout and volume, as well as, for given mass eruption rates, explaining in terms of eruption duration, the variable volumes and geometries expressed by variable aspect ratios.

In conclusion, after more than 20 years of focus on the local sedimentology of ignimbrites we think it is time to re-appraise the importance of first order geometric descriptors. These relate more properly to first order changes of source and flow mechanisms via variations in mass flow rate that cannot be captured simply by flow boundary models of sedimentation. Furthermore, while complex processes of local

sedimentation are presently approached mostly by analogue models, on the other end, sedimentation cannot be properly scaled to ignimbrite time- and length-scales. For these reasons, first order geometric descriptors for ignimbrites such as areal extent, volume, aspect ratios, thickness relationship to topography are important as they can be modeled numerically and may provide further understanding of pyroclastic current dynamics, especially for the large volume ignimbrites related to caldera forming super-eruptions that are certainly at present one of the least understood volcanic phenomena.

A major challenge for the future in physical field-volcanology is the accurate reconstruction of what is a single ignimbrite unit and how we measure/extrapolate its relevant first order-descriptors. Provided that accurate stratigraphic studies should be able to clearly identify single depositional/cooling units (defined as the deposit of a single and continuous flow event with no time breaks, irrespective of internal variations in deposit features due to pulses in eruption dynamics and local interaction with topography, and clearly bounded by top and bottom stratigraphic surfaces), the calculation of their volume, thicknesses and areal extent (just to mention the most commonly quoted quantities in the literature) has proven to be often aleatoric, because of the many and poorly defined ways proposed to make such measurements and extrapolations (see discussions in Mason et al., 2004; Folkes et al., 2011; Crosweller et al., 2012; Silleni et al., 2020). In the future, the volcanological community should focus on developing much more standardized ways of measuring such quantities, to reduce uncertainties and to make measurements reproducible, such as has been done for the description of fall deposits (e.g. Bonadonna et al., 2016).

Supplementary data to this article can be found online at https://doi.org/10.1016/j.earscirev.2021.103697.

References

Andrews, B.J., Manga, M., 2011. Effects of topography on pyroclastic density current runout and formation of coignimbrites. Geology 39 (12), 1099–1102.

Andrews, B.J., Manga, M., 2012. Experimental study of turbulence, sedimentation, and coignimbrite mass partitioning in dilute pyroclastic density currents. J. Volcanol. Geotherm. Res. 225, 30–44.

Bacon, C.R., 1983. Eruptive history of Mount Mazama and Crater Lake caldera, Cascade Range, USA. J. Volcanol. Geotherm. Res. 18 (1–4), 57–115.

Baer, E.M., Fisher, R.V., Fuller, M., Valentine, G., 1997. Turbulent transport and deposition of the Ito pyroclastic flow: determinations using anisotropy of magnetic susceptibility. Journal of Geophysical Research: Solid Earth 102 (B10), 22565–22586.

Báez, W., Arnosio, M., Chiodi, A., Ortiz-Yañes, A., Viramonte, J.G., Bustos, E., López, J.F., 2015. Estratigrafía y evolución del Complejo Volcánico Cerro Blanco, Puna Austral, Argentina. Revista mexicana de ciencias geológicas 32 (1), 29–49.

Báez, W., Bustos, E., Chiodi, A., Reckziegel, F., Arnosio, M., de Silva, S., Peña-Monné, J. L., 2020. Eruptive style and flow dynamics of the pyroclastic density currents related to the Holocene Cerro Blanco eruption (Southern Puna plateau, Argentina). J. S. Am. Earth Sci. 98, 102482.

Bear, A.N., Cas, R.A.F., Giordano, G., 2009. The implications of spatter, pumice and lithic clast rich proximal co-ignimbrite lag breccias on the dynamics of caldera forming eruptions: the 151 ka Sutri eruption, Vico Volcano, Central Italy. J. Volcanol. Geotherm. Res. 181 (1), 1–24.

Best, M.G., Christiansen, E.H., Deino, A.L., Gromme, S., Hart, G.L., Tingey, D.G., 2013. The 36 18 Ma Indian Peak Caliente ignimbrite field and calderas, southeastern Great Basin, USA: multicyclic super-eruptions. Geosphere 9 (4), 864–950.

Bonadonna, C., Costa, A., 2013. Plume height, volume, and classification of explosive volcanic eruptions based on the Weibull function. Bull. Volcanol. 75 (8), 1–19.

Bonadonna, C., Cioni, R., Costa, A., Druitt, T., Phillips, J., Pioli, L., Bagheri, G., 2016. MeMoVolc report on classification and dynamics of volcanic explosive eruptions. Bull. Volcanol. 78 (11), 84.

Brand, B.D., Mackaman-Lofland, C., Pollock, N.M., Bendaña, S., Dawson, B., Wichgers, P., 2014. Dynamics of pyroclastic density currents: Conditions that promote substrate erosion and self-channelization—Mount St Helens, Washington (USA). J. Volcanol. Geotherm. Res. 276, 189 214.

Brand, B.D., Bendaña, S., Self, S., Pollock, N., 2016. Topographic controls on pyroclastic density current dynamics: Insight from 18 May 1980 deposits at Mount St. Helens, Washington (USA). J. Volcanol. Geotherm. Res. 321, 1–17.

Branney, M., Acocella, V., 2015. Calderas. In: The Encyclopedia of Volcanoes, second edition. Academic Press, pp. 299 315.

Branney, M.J., Kokelaar, B.P., 2002. Pyroclastic density currents and the sedimentation of ignimbrites. Geological Society of London. Memoirs 27, 145.

Breard, E.C., Lube, G., 2017. Inside pyroclastic density currents–uncovering the enigmatic flow structure and transport behaviour in large-scale experiments. Earth Planet. Sci. Lett. 458, 22 36.

Breard, E.C., Dufek, J., Lube, G., 2018. Enhanced mobility in concentrated pyroclastic density currents: an examination of a self-fluidization mechanism. Geophys. Res. Lett. 45 (2), 654–664.

Brown, R.J., Andrews, G.D., 2015. Deposits of pyroclastic density currents. In: The Encyclopedia of Volcanoes. Academic Press, pp. 631–648.

Brown, S.K, Crosweller, H.S., Sparks, R.S.J., Cottrell, E., et al., 2014. Characterisation of the Quaternary eruption record: analysis of the Large Magnitude Explosive Volcanic Eruptions (LaMEVE) database. J. Appl. Volcanol. 3 (1), 1–22. https://doi.org/10.1186/2191-5040-3-5.

Bursik, M.I., Woods, A.W., 1996. The dynamics and thermodynamics of large ash flows. Bull. Volcanol. 58 (2–3), 175–193.

Cas, R.A.F., Wright, J.V., 1987. Volcanic Successions: Ancient and Modern. Allen and Unin, London.

Cas, R.A.F., Wright, H.M., Folkes, C.B., Lesti, C., Porreca, M., Giordano, G., Viramonte, J. G., 2011. The flow dynamics of an extremely large volume pyroclastic flow, the 2.08-Ma Cerro Galán Ignimbrite, NW Argentina, and comparison with other flow types. Bull. Volcanol. 73 (10), 1583–1609.

Cashman, K.V., Giordano, G., 2014. Calderas and magma reservoirs. J. Volcanol. Geotherm. Res. 288, 28–45.

Castruccio, A., Clavero, J., Segura, A., Samaniego, P., Roche, O., Le Pennec, J.L., Droguett, B., 2016. Eruptive parameters and dynamics of the April 2015 sub-Plinian eruptions of Calbuco volcano (southern Chile). Bull. Volcanol. 78 (9), 62.

Chesner, C.A., Rose, W.I., 1991. Stratigraphy of the Toba tuffs and the evolution of the Toba caldera complex, Sumatra, Indonesia. Bull. Volcanol. 53 (5), 343–356.

Cioni, R., Bertagnini, A., Santacroce, R., Andronico, D., 2008. Explosive activity and eruption scenarios at Somma-Vesuvius (Italy): towards a new classification scheme. J. Volcanol. Geotherm. Res. 178 (3), 311–346.

Cole, P.D., Calder, E.S., Sparks, R.S.J., Clarke, A.B., Druitt, T.H., Young, S.R., Norton, G. E., 2002. Deposits from dome-collapse and fountain-collapse pyroclastic flows at Soufrière Hills Volcano, Montserrat. Geological Society, London, Memoirs 21 (1), 231–262.

Cole, J.W., Milner, D.M., Spinks, K.D., 2005. Calderas and caldera structures: a review. Earth Sci. Rev. 69 (1 2), 1 26.

Costa, A., Smith, V., Macedonio, G., Matthews, N., 2014. The magnitude and impact of the Youngest Toba Tuff super-eruption. Front. Earth Sci. 2, 16.

Costa, A., Suzuki, Y., Koyaguchi, T., 2018. Understanding the plume dynamics of explosive super-eruptions. Nat. Commun. 9 (1), 654.

Crosweller, H.S., Arora, B., Brown, S.K., Cottrell, E., Deligne, N.I., Guerrero, N.O., Nayembil, M., 2012. Global database on large magnitude explosive volcanic eruptions (LaMEVE). J. Appl. Volcanol. 1 (1), 4.

Dade, W.B., Huppert, H.E., 1996. Emplacement of the Taupo ignimbrite by a dilute turbulent flow. Nature 381 (6582), 509–512.

De Rita, D., Giordano, G., Milli, S., 1998. Forestepping-backstepping stacking pattern of volcaniclastic successions: Roccamonfina volcano, Italy. J. Volcanol. Geotherm. Res. 80 (1–2), 155–178.

de Silva, S.L., Gregg, P.M., 2014. Thermomechanical feedbacks in magmatic systems: Implications for growth, longevity, and evolution of large caldera-forming magma reservoirs and their supereruptions. J. Volcanol. Geotherm. Res. 282, 77 91.

de Silva, S., Zandt, G., Trumbull, R., Viramonte, J.G., Salas, G., Jiménez, N., 2006. Large ignimbrite eruptions and volcano-tectonic depressions in the Central Andes: a thermomechanical perspective. Geol. Soc. Lond., Spec. Publ. 269 (1), 47–63.

Dobran, F., Neri, A., Macedonio, G., 1993. Numerical simulation of collapsing volcanic columns. Journal of Geophysical Research: Solid Earth 98 (B3), 4231–4259.

Doronzo, D.M., 2012. Two new end members of pyroclastic density currents: forced convection-dominated and inertia-dominated. J. Volcanol. Geotherm. Res. 219, 87–91.

Doronzo, D.M., Martí, J., Dellino, P., Giordano, G., Sulpizio, R., 2016. Dust storms, volcanic ash hurricanes, and turbidity currents: physical similarities and differences with emphasis on flow temperature. Arab. J. Geosci. 9 (4), 1–9.

Druitt, T.H., Bacon, C.R., 1986. Lithic breccia and ignimbrite erupted during the collapse of Crater Lake Caldera, Oregon. J. Volcanol. Geotherm. Res. 29 (1–4), 1–32.

Druitt, T.H., Sparks, R.S.J., 1984. On the formation of calderas during ignimbrite eruptions. Nature 310 (5979), 679–681.

Druitt, T.H., Young, S.R., Baptie, B., Bonadonna, C., Calder, E.S., Clarke, A.B., Ryan, G., 2002. Episodes of cyclic Vulcanian explosive activity with fountain collapse at Soufrière Hills Volcano, Montserrat. Memoirs-Geological Society of London 21, 281–306.

Dufek, J., 2016. The fluid mechanics of pyroclastic density currents. Annu. Rev. Fluid Mech. 48, 459–485.

Dufek, J., Bergantz, G.W., 2007. Dynamics and deposits generated by the Kos Plateau Tuff eruption: Controls of basal particle loss on pyroclastic flow transport. Geochemistry, Geophysics, Geosystems 8 (12).

Dufek, J., Esposti Ongaro, T., Roche, O., 2015. Pyroclastic density currents: Processes and models. In: The Encyclopedia of Volcanoes, Second edition. Academic Press, pp. 617 629.

Esposti Ongaro, T., Neri, A., Menconi, G., Vitturi, M.D.M., Marianelli, P., Cavazzoni, C., Baxter, P.J., 2008. Transient 3D numerical simulations of column collapse and pyroclastic density current scenarios at Vesuvius. J. Volcanol. Geotherm. Res. 178 (3), 378–396.

Esposti Ongaro, T., Komorowski, J.C., Legendre, Y., Neri, A., 2020. Modelling pyroclastic density currents from a subplinian eruption at La Soufrière de Guadeloupe (West Indies, France). Bull. Volcanol. 82 (12), 1–26.

Fierstein, J., Hildreth, W., 1992. The plinian eruptions of 1912 at Novarupta, Katmai National Park, Alaska. Bull. Volcanol. 54, 646–684.

Fisher, R.V., 1966. Mechanism of deposition from pyroclastic flows. Am. J. Sci. 264 (5), 350–363.

Fisher, R.V., 1995. Decoupling of pyroclastic currents: hazards assessments. J. Volcanol. Geotherm. Res. 66 (1–4), 257–263.

Fisher, R.V., Orsi, G., Ort, M., Heiken, G., 1993. Mobility of a large-volume pyroclastic flow—emplacement of the Campanian ignimbrite, Italy. J. Volcanol. Geotherm. Res. 56 (3), 205–220.

Folkes, C.B., Wright, H.M., Cas, R.A., de Silva, S.L., Lesti, C., Viramonte, J.G., 2011. A re-appraisal of the stratigraphy and volcanology of the Cerro Galán volcanic system, NW Argentina. Bull. Volcanol. 73 (10), 1427–1454.

Freundt, A., Wilson, C.J.N., Carey, S.N., 2000. Ignimbrites and block-and-ash flow deposits. In: Sigurdsson, et al. (Eds.), Encyclopedia of Volcanoes. Academic Press.

Fujii, T., Nakada, S., 1999. The 15 September 1991 pyroclastic flows at Unzen Volcano (Japan): a flow model for associated ash-cloud surges. J. Volcanol. Geotherm. Res. 89 (1–4), 159–172.

Geshi, N., Ruch, J., Acocella, V., 2014. Evaluating volumes for magma chambers and magma withdrawn for caldera collapse. Earth Planet. Sci. Lett. 396, 107–115.

Geyer, A., Marti, J., 2008. The new worldwide collapse caldera database (CCDB): a tool for studying and understanding caldera processes. J. Volcanol. Geotherm. Res. 175 (3), 334–354.

Geyer, A., Folch, A., Martí, J., 2006. Relationship between caldera collapse and magma chamber withdrawal: an experimental approach. J. Volcanol. Geotherm. Res. 157 (4), 375–386.

Giordano, G., 1998. The effect of paleotopography on lithic distribution and facies associations of small volume ignimbrites: the WTT Cupa (Roccamonfina volcano, Italy). J. Volcanol. Geotherm. Res. 87 (1–4), 255–273.

Giordano, G., De Astis, G., 2021. The summer 2019 basaltic Vulcanian eruptions (paroxysms) of Stromboli. Bull. Volcanol. 83, 1. https://doi.org/10.1007/s00445-020-01423-2.

Giordano, G., Dobran, F., 1994. Computer simulations of the Tuscolano Artemisio's second pyroclastic flow unit (Alban Hills, Latium, Italy). J. Volcanol. Geotherm. Res. 61 (1–2), 69–94.

Giordano, G., Doronzo, D., 2017. Sedimentation and mobility of PDCs: a reappraisal of ignimbrites' aspect ratio. Sci. Rep. 7, 4444. https://doi.org/10.1038/s41598-017-04880-6.

Giordano, G., De Rita, D., Cas, R., Rodani, S., 2002. Valley pond and ignimbrite veneer deposits in the small-volume phreatomagmatic 'Peperino Albano' basic ignimbrite, Lago Albano maar, Colli Albani volcano, Italy: influence of topography. J. Volcanol. Geotherm. Res. 118 (1 2), 131 144.

Giordano, G., The CARG Team, 2010. Stratigraphy, volcano tectonics and evolution of the Colli Albani volcanic field. The Colli Albani Volcano: Geological Society, London, Special Publications of IAVCEI 3, 43–98.

Gregg, P.M., De Silva, S.L., Grosfils, E.B., Parmigiani, J.P., 2012. Catastrophic caldera-forming eruptions: Thermomechanics and implications for eruption triggering and maximum caldera dimensions on Earth. J. Volcanol. Geotherm. Res. 241, 1–12.

Hildreth, W., Fierstein, J., 2012. The Novarupta-Katmai Eruption of 1912: Largest Eruption of the Twentieth Century: Centennial Perspectives. US Geol. Surv. Prof. Pap. 1791, 1–256.

Hildreth, W., Mahood, G.A., 1986. Ring-fracture eruption of the Bishop Tuff. Geol. Soc. Am. Bull. 97 (4), 396–403.

Jessop, D.E., Gilchrist, J., Jellinek, A.M., Roche, O., 2016. Are eruptions from linear fissures and caldera ring dykes more likely to produce pyroclastic flows? Earth Planet. Sci. Lett. 454, 142–153.

Kelfoun, K., Samaniego, P., Palacios, P., Barba, D., 2009. Testing the suitability of frictional behaviour for pyroclastic flow simulation by comparison with a well-constrained eruption at Tungurahua olcano (Ecuador). Bull. Volcanol. 71 (1057–7).

Kennedy, B., Stix, J., Vallance, J.W., Lavallée, Y., Longpré, M.A., 2004. Controls on caldera structure: results from analogue sandbox modeling. Geol. Soc. Am. Bull. 116 (5–6), 515–524.

Lavallée, Y., Wadsworth, F.B., Vasseur, J., Russell, J.K., Andrews, G.D., Hess, K.U., Dingwell, D.B., 2015. Eruption and emplacement timescales of ignimbrite super-eruptions from thermo-kinetics of glass shards. Front. Earth Sci. 3, 2.

Lesti, C., Porreca, M., Giordano, G., Mattei, M., Cas, R.A., Wright, H.M., Viramonte, J., 2011. High-temperature emplacement of the Cerro Galán and Toconquis Group ignimbrites (Puna plateau, NW Argentina) determined by TRM analyses. Bull. Volcanol. 73 (10), 1535–1565.

Lindsay, J.M., Schmitt, A.K., Trumbull, R.B., De Silva, S.L., Siebel, W., Emmermann, R., 2001. Magmatic evolution of the La Pacana caldera system, Central Andes, Chile: Compositional variation of two cogenetic, large-volume felsic ignimbrites. J. Petrol. 42 (3), 459 486.

Lipman, P.W., 1997. Subsidence of ash-flow calderas: relation to caldera size and magma-chamber geometry. Bull. Volcanol. 59 (3), 198–218.

Lube, G., Cronin, S.J., Platz, T., Freundt, A., Procter, J.N., Henderson, C., Sheridan, M.F., 2007. Flow and deposition of pyroclastic granular flows: a type example from the 1975 Ngauruhoe eruption, New Zealand. J. Volcanol. Geotherm. Res. 161 (3), 165–186.

Lube, G., Breard, E.C., Esposti-Ongaro, T., Dufek, J., Brand, B., 2020. Multiphase flow behaviour and hazard prediction of pyroclastic density currents. Nature Reviews Earth & Environment 1–18.

Major, J.J., Pierson, T.C., Hoblitt, R.P., Moreno, H., 2013. Pyroclastic density currents associated with the 2008-2009 eruption of Chaitén Volcano (Chile): Forest disturbances, deposits, and dynamics. Andean Geol. 40 (2), 324–358.

Mason, B.G., Pyle, D.M., Oppenheimer, C., 2004. The size and frequency of the largest explosive eruptions on Earth. Bull. Volcanol. 66 (8), 735–748.

Maughan, L.L., Christiansen, E.H., Best, M.G., Gromme, C.S., Deino, A.L., Tingey, D.G., 2002. The Oligocene Lund Tuff, Great Basin, USA: a very large volume monotonous intermediate. J. Volcanol. Geotherm. Res. 113 (1), 129–157.

Miller, C.F., Wark, D.A., 2008. Supervolcanoes and their explosive supereruptions. Elements 4 (1), 11–15.

Milner, D.M., Cole, J.W., Wood, C.P., 2003. Mamaku Ignimbrite: a caldera-forming ignimbrite erupted from a compositionally zoned magma chamber in Taupo Volcanic Zone, New Zealand. J. Volcanol. Geotherm. Res. 122 (3–4), 243–264.

Nairn, I.A., Self, S., 1978. Explosive eruptions and pyroclastic avalanches from Ngauruhoe in February 1975. J. Volcanol. Geotherm. Res. 3 (1–2), 39–60.

Newhall, C.G., Self, S., 1982. The volcanic explosivity index (VEI) an estimate of explosive magnitude for historical volcanism. Journal of Geophysical Research: Oceans 87 (C2), 1231–1238.

Ort, M.H., Orsi, G., Pappalardo, L., Fisher, R.V., 2003. Anisotropy of magnetic susceptibility studies of depositional processes in the Campanian Ignimbrite, Italy. Bull. Volcanol. 65 (1), 55 72.

Palladino, D.M., 2017. Simply pyroclastic currents. Bull. Volcanol. 79 (7), 53.

Palladino, D.M., Giordano, G., 2019. On the mobility of pyroclastic currents in light of deposit thickness and clast size trends. J. Volcanol. Geotherm. Res. 384, 64–74.

Palladino, D.M., Valentine, G.A., 1995. Coarse-tail vertical and lateral grading in pyroclastic flow deposits of the Latera Volcanic complex (Vulsini, Central Italy): origin and implications for flow dynamics. J. Volcanol. Geotherm. Res. 69 (3–4), 343–364.

Palladino, D.M., Simei, S., Sottili, G., Trigila, R., 2010. Integrated approach for the reconstruction of stratigraphy and geology of quaternary volcanic terrains: an application to the Vulsini Volcanoes (Central Italy). In: Groppelli G, Viereck-Goette L (eds) Stratigraphy and Geology of Volcanic areas. Geol Soc Am Sp Pap 464, 63–84. https://doi.org/10.1130/2010.2464(04).

Pensa, A., Cas, R., Giordano, G., Porreca, M., Wallenstein, N., 2015. Transition from steady to unsteady Plinian eruption column: the VEI 5, 4.6 ka Fogo a Plinian eruption, São Miguel, Azores. J. Volcanol. Geotherm. Res. 305, 1–18.

Pinel, V., Jaupart, C., 2005. Caldera formation by magma withdrawal from a reservoir beneath a volcanic edifice. Earth Planet. Sci. Lett. 230 (3), 273–287.

Pittari, A., Cas, R.A.F., Edgar, C.J., Nichols, H.J., Wolff, J.A., Martí, J., 2006. The influence of palaeotopography on facies architecture and pyroclastic flow processes of a lithic-rich ignimbrite in a high gradient setting: the Abrigo Ignimbrite, Tenerife, Canary Islands. *Journal of Volcanology and Geothermal Research*, *152*(3-4), 273-315.

Pyle, D.M., 1989. The thickness, volume and grainsize of tephra fall deposits. Bull. Volcanol. 51, 1 15.

Pollock, N.M., Brand, B.D., Rowley, P.J., Sarocchi, D., Sulpizio, R., 2019. Inferring pyroclastic density current flow conditions using syn-depositional sedimentary structures. Bull. Volcanol. 81 (8), 1–16. https://doi.org/10.1007/s00445-019-1303-z.

Pyle, D.M., 2015. Sizes of volcanic eruptions. In: The Encyclopedia of Volcanoes. Academic Press, pp. 257–264.

Quane, S.L., Russell, J.K., 2005. Ranking welding intensity in pyroclastic deposits. Bull. Volcanol. 67 (2), 129–143.

Rampino R, M, 2002. Supereruptions as a threat to civilizations on Earth-like planets. Icarus 156 (2), 562 569. https://doi.org/10.1006/icar.2001.6808.

Roche, O., Druitt, T.H., 2001. Onset of caldera collapse during ignimbrite eruptions. Earth Planet. Sci. Lett. 191 (3), 191–202.

Roche, O., Druitt, T.H., Merle, O., 2000. Experimental study of caldera formation. Journal of Geophysical Research: Solid Earth 105 (B1), 395–416.

Roche, O., Buesch, D.C., Valentine, G.A., 2016. Slow-moving and far-travelled dense pyroclastic flows during the Peach Spring super-eruption. Nature communications 7.

Romano, C., Vona, A., Campagnola, S., Giordano, G., Arienzo, I., Isaia, R., 2020. Modelling and physico-chemical constraints to the 4.5 ka Agnano-Monte Spina Plinian eruption (Campi Flegrei, Italy). Chem. Geol. 532, 119301.

Romero, J.E., Morgavi, D., Arzilli, F., Daga, R., Caselli, A., Reckziegel, F., Perugini, D., 2016. Eruption dynamics of the 22–23 April 2015 Calbuco Volcano (Southern Chile): analyses of tephra fall deposits. J. Volcanol. Geotherm. Res. 317, 15–29.

Rosi, M., Sbrana, A., Principe, C., 1983. The Phlegraean Fields: structural evolution, volcanic history and eruptive mechanisms. J. Volcanol. Geotherm. Res. 17 (1–4), 273–288.

Rowley, P.D., 1981. Pyroclastic-flow deposits. The 1980 eruptions of Mount St. Helens, Washington. US Geol. Surv. Prof. Paper 1250, 489–512.

Scott, W.E., Hoblitt, R.P., Torres, R.C., Self, S., Martinez, M.M.L., Nillos, T., 1996. Pyroclastic flows of the June 15, 1991, climactic eruption of Mount Pinatubo. Fire and Mud: eruptions and lahars of Mount Pinatubo, Philippines 545–570.

Self, S., Goff, F., Gardner, J.N., Wright, J.V., Kite, W.M., 1986. Explosive rhyolitic volcanism in the Jemez Mountains: vent locations, caldera development and relation to regional structure. Journal of Geophysical Research: Solid Earth 91 (B2), 1779–1798.

Shimizu, H.A., Koyaguchi, T., Suzuki, Y.J., 2019. The run-out distance of large-scale pyroclastic density currents: a two-layer depth-averaged model. J. Volcanol. Geotherm. Res. 381, 168–184.

Sigurdsson, H., Carey, S., Cornell, W., Pescatore, T., 1985. The eruption of Vesuvius in a. D. 79. Natl. Geogr. Res. 1, 332–387.

Silleni, A., Giordano, G., Isaia, R., Ort, M.H., 2020. Magnitude of the 39.8 ka Campanian Ignimbrite Eruption, Italy: method, uncertainties and errors. Front. Earth Sci. 8, 444.

Simmons, J.M., Cas, R.A.F., Druitt, T.H., Folkes, C.B., 2016. Complex variations during a caldera-forming Plinian eruption, including precursor deposits, thick pumice fallout, co-ignimbrite breccias and climactic lag breccias: the 184 ka lower Pumice 1 eruption sequence, Santorini, Greece. J. Volcanol. Geotherm. Res. 324, 200–219.

Smith, R.L., 1960a. Ash flows. Geol. Soc. Am. Bull. 71 (6), 795–841.

Smith, R.L., 1960b. Zones and zonal variations in welded ash flows. Geol Soc Am Prof Paper 354-F, 149 159.

Smith, R.L., 1979. Ash-flow magmatism. Geol. Soc. Am. Spec. Pap. 180, 5–28.

Smith, R.L., Bailey, R.A., 1968. Resurgent cauldrons. Memoir of the Geological Society of America 116, 613–662.

Smith, G., Rowley, P., Williams, R., Giordano, G., Trolese, M., Silleni, A., Capon, S., 2020. A bedform phase diagram for dense granular currents. Nat. Commun. 11 (1), 1–11.

Sparks, R.S.J., 1975. Stratigraphy and geology of the ignimbrites of Vulsini Volcano, Central Italy. Geol. Rundsch. 64 (1), 497–523.

Sparks, R.S.J., 1976. Grain size variations in ignimbrites and implications for the transport of pyroclastic flows. Sedimentology 23 (2), 147–188.

Sparks, R.S.J., Self, S., Walker, G.P., 1973. Products of ignimbrite eruptions. Geology 1 (3), 115–118.

Sparks, R.S.J., Wilson, L., Hulme, G., 1978. Theoretical modeling of the generation, movement, and emplacement of pyroclastic flows by column collapse. Journal of Geophysical Research: Solid Earth 83 (B4), 1727–1739.

Streck, M.J., Grunder, A.L., 1995. Crystallization and welding variations in a widespread ignimbrite sheet; the Rattlesnake Tuff, eastern Oregon, USA. Bull. Volcanol. 57 (3), 151–169.

Sulpizio, R., Mele, D., Dellino, P., La Volpe, L., 2007. Deposits and physical properties of pyroclastic density currents during complex Subplinian eruptions: the AD 472 (Pollena) eruption of Somma-Vesuvius, Italy. Sedimentology 54 (3), 607 635.

Sulpizio, R., Dellino, P., Doronzo, D.M., Sarocchi, D., 2014. Pyroclastic density currents: state of the art and perspectives. J. Volcanol. Geotherm. Res. 283, 36–65.

Suzuki, Y.J., Koyaguchi, T., Ogawa, M., Hachisu, I., 2005. A numerical study of turbulent mixing in eruption clouds using a three-dimensional fluid dynamics model. Journal of Geophysical Research: Solid Earth 110 (B8).

Trolese, Matteo, Cerminara, Matteo, Esposti Ongaro, Tomaso, Giordano, Guido, 2019. The footprint of column collapse regimes on pyroclastic flow temperatures and plume heights. Nature Comm. 10 (1), 1 10. https://doi.org/10.1038/s41467-019-10337-3, 2476.

Trolese, M., Giordano, G., Cifelli, F., Winkler, A., Mattei, M., 2017. Forced transport of thermal energy in magmatic and phreatomagmatic large volume ignimbrites: Paleomagnetic evidence from the Colli Albani volcano, Italy. Earth Planet. Sci. Lett. 478, 179 191.

Valentine, G.A., Fisher, R.V., 2000. Pyroclastic Surges and Blasts. (Encyclopedia of Volcanoes).

Valentine, G.A., Wohletz, K.H., 1989. Numerical models of Plinian eruption columns and pyroclastic flows. J. Geophys. Res. 94 (B2), 1867–1887.

Vinkler, A.P., Cashman, K., Giordano, G., Groppelli, G., 2012. Evolution of the mafic Villa Senni caldera-forming eruption at Colli Albani volcano, Italy, indicated by textural analysis of juvenile fragments. J. Volcanol. Geotherm. Res. 235, 37–54.

Vona, A., Romano, C., Giordano, D., Sulpizio, R., 2020. Linking magma texture, rheology and eruptive style during the 472 AD Pollena Subplinian eruption (Somma-Vesuvius). Lithos 370, 105658.

Walker, G.P.L., 1973. Explosive volcanic eruptions —a new classification scheme. Geol. Rundsch. 62, 431–446.

Walker, G.P., 1983. Ignimbrite types and ignimbrite problems. J. Volcanol. Geotherm. Res. 17 (1–4), 65–88.

Walker, G.P.L., Heming, R.F., Wilson, C.J.N., 1980. Low-aspect ratio ignimbrites. Nature 283 (5744), 286–287.

Willcock, M.A.W., Cas, R.A.F., Giordano, G., Morelli, C., 2013. The eruption, pyroclastic flow behaviour, and caldera in-filling processes of the extremely large volume (> 1290km 3), intra-to extra-caldera, Permian Ora (ignimbrite) Formation, southern Alps, Italy. J. Volcanol. Geotherm. Res. 265, 102–126.

Wilson, C.J.N., 1991. Ignimbrite morphology and the effects of erosion: a New Zealand case study. Bull. Volcanol. 53 (8), 635–644.

Wilson, C.J.N., 2001. The 26.5 ka Oruanui eruption, New Zealand: an introduction and overview. J. Volcanol. Geotherm. Res. 112 (1–4), 133–174.

Wilson, C.J.N., 2008. Supereruptions and supervolcanoes: processes and products. Elements 4 (1), 29–34.

Wilson, C.J., Hildreth, W., 1997. The Bishop Tuff: new insights from eruptive stratigraphy. The Journal of Geology 105 (4), 407–440.

Wilson, C.J.N., Hildreth, W., 2003. Assembling an ignimbrite: Mechanical and thermal building blocks in the Bishop Tuff, California. The Journal of Geology 111 (6), 653–670.

Wilson, C.J.N., Walker, G.P., 1985. The Taupo eruption, New Zealand I. General aspects. Philosophical Transactions of the Royal Society of London A: Mathematical, Physical and Engineering Sciences 314 (1529), 199–228.

Wilson, L., Sparks, R.S.J., Walker, G.P., 1980. Explosive volcanic eruptions—IV. The control of magma properties and conduit geometry on eruption column behaviour. Geophys. J. Int. 63 (1), 117 148.

Wilson, C.J.N., Houghton, B.F., Kamp, P.J.J., McWilliams, M.O., 1995. An exceptionally widespread ignimbrite with implications for pyroclastic flow emplacement. Nature 378 (6557), 605.

Wohletz, K.H., Sheridan, M.F., 1979. A model for pyroclastic surges. Geol. Soc. Am. Spec. Pap. 180, 177–194.

Zrelak, P.J., Pollock, N.M., Brand, B.D., Sarocchi, D., Hawkins, T., 2020. Decoding pyroclastic density current flow direction and shear conditions in the flow boundary zone via particle-fabric analysis. J. Volcanol. Geotherm. Res. 402, 106978.